NASA Contractor Report 178036

AN INVESTIGATION AT STATIC CONDITIONS OF NONAXISYMMETRIC NOZZLE THRUST REVERSER PORT GEOMETRY INCLUDING EFFECTS OF ROUNDING AND ROTATING THE PORT CORNER

Dorothy G. Arbiter

VIGYAN RESEARCH ASSOCIATES, INC.
Hampton, Virginia 23666

Contract NAS1-17919
November 1985

National Aeronautics and Space Administration

Langley Research Center
Hampton, Virginia 23665

TABLE OF CONTENTS

SYMBOLS

A_e - nozzle axit area, in^2

A_t - port geometric throat area, in^2

A^* - effective nozzle throat area, in^2

F - axial thrust component, lb_f

F_i - ideal isentropic gross thrust, lb_f

F_n - normal thrust component, lb_f

F_r - resultant gross thrust, $\sqrt{F^2 + F_n^2}$, lb_f

NPR - nozzle pressure ratio, $P_{t,j}/P_a$

P_a - ambient pressure, psi

$P_{t,j}$ - jet total pressure, psi

RPM - revolutions per minute, 1/min

w_p - measured mass-flow rate, slugs/s

w_p/w_i - discharge coefficient, no units

w_i - ideal mass-flow rate, slugs/s

β - blocker angle, degrees

δ - resultant thrust vector angle, $\tan^{-1} \frac{F_n}{F}$, degrees

ABBREVIATIONS

CW - clockwise

CCW - counterclockwise

conf. - configuration

M.S. - model station

ref. - reference

2-D C-D - two-dimensional convergent-divergent

LIST OF FIGURES

TABLE

FIGURE

CHAPTER I

INTRODUCTION

Requirements for the next generation of fighter aircraft will probably include short take-off and landing capabilities, an expanded maneuver envelope, and an integrated flight and propulsion control system (refs. 1-4). These aircraft may require exhaust nozzles capable of thrust vectoring and thrust reversing to help meet these demands. Towards achieving these goals, many advanced exhaust nozzle models have been designed and tested to determine internal and installed performance (refs. 5-21). These nozzle models can be divided into two groups: advanced axisymmetric and nonaxisymmetric. Exhaust nozzle internal performance studies indicate that nonaxisymmetric nozzles have essentially the same level of internal performance as conventional axisymmetric nozzles (refs. 10, 12, 13, 15, 16, 18, 19). Nonaxisymmetric nozzles have an advantage over axisymmetric nozzles because their two-dimensional shape can more easily incorporate thrust vectoring and reversing, providing additional capability for the lowest weight penalty (refs. 22-28). Factors such as internal performance, external drag, weight, cooling, and vectoring/reversing requirements become the basis for determining the best nozzle for a particular application. Further, the effects of the vectoring/reversing on the airframe and engine must be determined.

Before new technology can be incorporated, the effects of integrating it into a system must be explored. Performance tests indicate that current exhaust nozzle thrust reverser models can be designed to obtain the desired amounts of reverse thrust but often fail to maintain the mass flow rate that would be required by the engine to prevent engine stall (refs. 14, 19, 21, 28). The results of an investigation to determine the internal flow characteristics of a typical two-dimensional thrust reverser model (ref. 29) indicated that the

sonic lines in the thrust reverser ports were highly inclined. Evidence of exhaust flow separation along the upstream port wall was also presented. These results indicate that an effective port throat area smaller than the geometric port throat area may be the cause of the low mass-flow rate (low discharge coefficient) during reverse thrust operation when compared to the normal mass-flow rate of the nozzle during cruise.

To prevent engine stall during reverser deployment, some minimum change in mass-flow rate (generally less than 8- to 10-percent) must be maintained. Two options are available to the designer. Either a reverser-port variable-area control device must be incorporated into the exhaust nozzle hardware to increase the geometric port throat area (inversely proportional to the decrease in effective port throat area), or the internal geometry of the thrust reverser must be modified to increase port discharge coefficient (increase effective port throat area). The purpose of this investigation was to determine the effects on internal performance of first, rounding the upstream corner of the reverser port entrance (most current configurations have sharp or angular corners), and second, incorporating a rotating cylinder into the corner of several thrust reverser port configurations. Except for the port corner modifications, the nozzle hardware was identical to the model presented in reference 28. Some configurations reported in reference 28 were retested to insure consistency of the data for the current investigation. The tests were conducted in the static test facility of the NASA Langley 16-Foot Transonic Tunnel. A temperature controlled, high pressure air system was used to simulate engine exhaust at nozzle pressure ratios up to 6.0.

CHAPTER II

APPARATUS AND PROCEDURES

Facility Description

The tests were conducted in the static test facility associated with the NASA Langley 16-Foot Transonic Tunnel. Engine exhaust was simulated by a high pressure air system with a heat exchanger to control air temperature. The nozzle exhaust was vented to atmosphere out a large door or towards a high ceiling depending on the nozzle configuration. A remotely located control room contained the air control valves and a closed circuit television monitor focused on the model. Data were recorded on a 96 channel, magnetic tape, data acquisition system.

Propulsion Simulator

The propulsion simulator used for this investigation was a single-engine air-powered nacelle model shown in the sketch of figure 1 with a typical thrust reverser port model installed. The body shell forward of model station (M.S.) 20.50 was removed for these tests. High pressure air maintained at an approximately constant temperature of 532° R was ducted into a high pressure plenum in the nonmetric (not on the balance) portion of the model. From the high pressure plenum, the air was discharged radially through eight equally-spaced sonic nozzles into the metric (on the balance) low pressure plenum. This system was designed to minimize the forces due to axial momentum when transferring the air from the nonmetric to the metric portion of the model. The flexible metal bellows shown in figure 1 were used as seals between the nonmetric and metric parts and compensated for axial forces caused by pressurization (ref. 30). Near the aft end of the low pressure plenum, the transition was made from a round duct to a rectangular passage cross-section. The air then passed through

a choke plate, an instrumentation section, and into the nozzle configuration at M.S. 41.13.

Nozzle Design

The model hardware downstream of M.S. 41.13 (see fig. 1) was used throughout the tests and simulated the upper half (one reverser port) of a two-dimensional convergent-divergent (2-D C-D) nozzle thrust reverser. Typically, a 2-D C-D nozzle thrust reverser is designed to reverse the flow upstream of the cruise or forward thrust mode throat (refs. 9, 11, 14-16, 18, 19, 23, 25). During thrust reverser deployment, the normal aft exhaust flow path is blocked and thrust reversing ports are opened on the upper and lower surfaces of the nozzle. The model hardware was designed to simulate only one reverser port in order to facilitate measurement of the normal component of thrust. Normal force of a symmetrical 2-D C-D thrust reverser with two reverser ports would equal zero. Measuring the normal force allowed straightforward calculation of resultant thrust (F_r) and thrust vector angle (δ). In order to simulate more closely the flow pattern of a 2-D C-D thrust reverser with two reverser ports, a splitter plate (leading edge at M.S. 42.33 and upper surface at nozzle centerline) was used to simulate the centerline of a thrust reverser restricting the exhaust flow to the flow path of a reverser with two ports.

Sketches of representative configurations of the three major port corner types tested (solid, rotating cylinder, and self-propelled rotating cylinder) are shown in figure 2. All configurations had a constant flow path width downstream of M.S. 41.13 of 4.00 inches. Most current nonaxisymmetric nozzle thrust reverser port designs have sharp or angular corners on the upstream port wall (refs. 14-16, 19). The purpose of the rounded port corner and the rotating cylinders shown in figure 2 was to eliminate the flow separation at the upstream port corner discussed in reference 14, 19 and 29. A representative solid round

corner configuration is shown in figure 2(a). Except for the rounded port corner, this design is typical of current 2-D C-D blocker type thrust reversers. A sketch of a typical 2-D C-D blocker type thrust reverser with a driven rotating cylinder located at the port corner is shown in figure 2(b). This sketch shows the sidewall location of the two motors used to drive the cylinder on many of the test configurations. Flexible metal couplings were used to connect the motors to the cylinder. The couplings corrected for any small misalignments between the cylinder and the motor shafts. Two precision bearings separated by a spacer were pressed into each nozzle sidewall. A magnetic sensor attached to the motor mount of the air driven motor was used to determine the revolutions per minute (RPM) of the rotating cylinder. The electric motor was a direct current motor with a maximum rotational speed of approximately 10,000 RPM when no load was on the cylinder. By reversing the direct current to the motor, cylinder rotation could be changed from the normal counterclockwise (CCW) direction (when model is viewed from the left side) to a clockwise (CW) direction. The air driven motor had an RPM range of 10,000 to 100,000 with no load on the cylinder. Because of problems associated with loads on the rotating cylinder during thrust reverser operation, no data were obtained with the cylinder driven by the air motor alone. A discussion of the cylinder rotational speeds obtained during the tests is contained in the Appendix.

The third type of port corner configuration utilized a larger port corner cylinder (see fig. 2(c)) and was designed to be self-propelled. Two different cylinder designs were tested. One cylinder had fins (similar to a waterwheel) located on the model centerline and the other cylinder had two sets of fins located at the ends of the rotating cylinder (see fig. 2(c)). The total surface area of the fins for the two cylinders was equal since the width of single set was the same as the total of the double set. A magnetic sensor located in the port corner over the cylinder fins (note alternate location for side fins,

fig. 2(c)) was used to determine the self-propelled rotating cylinder speed. The large cylinder port corners were designed to determine the effect of a self-propelled cylinder on the internal performance of the reverser port.

Geometric details of the port corner configurations tested are shown in figure 3. Details of the port corner configurations are summarized in Table I. All of the configurations were designed to obtain a geometric reverse thrust vector angle of 120 degrees. The blocker face (except for several alternate configurations) and the port upstream and downstream walls (port flow path) were all angled 120 degrees. Resultant thrust vector angle δ was measured from the horizontal reference line and δ = 0 degrees represented the cruise or forward thrust operating mode. Theoretically, a geometric reverse thrust angle of 120 degrees will provide a 50-percent component of resultant gross thrust (F_r) in the axial reverse thrust (F) direction ($F = F_r \cos 120 = -.5F_r$). All configurations tested were designed to have the same port throat area (A_t). Physical port throat dimensions were measured during the tests to determine the actual A_t (see Table I) for each configuration. Measured values of A_t were used in the data reduction procedures.

The solid round corner configurations (fig. 3(a)) and their rotating cylinder equivalents (fig. 3(b)) represented two types of thrust reverser internal geometry. Configurations 1 and 4 simulated a thrust reversing port located downstream of a constant area duct similar to those reported in references 16 and 19. Configurations 2, 3, and 5-7 represented thrust reverser ports located in the convergent portion of a nozzle and resembled those reported in reference 14. Each port corner (or cylinder) had a radius of 0.109 inches. Configurations 5 and 7 were used to investigate the effect of port passage length. The large cylinder port corners (see fig. 3(c) and 3(d)) all used cylinders with a radius of 0.250 inches. The parameters that varied for the large cylinder configurations

included cylinder fin location (see fig. 2(c)), downstream exit wall height, and internal blocker angle β.

Instrumentation

Jet total temperature and jet total pressure were measured by a single total-temperature probe and nine total-pressure probes located in the instrumentation section of the propulsion simulator (fig. 1). The nine total-pressure probes were attached to three rakes which were all located in the same passage cross-sectional plane. An area-weighted average of the individual probe total-pressure measurements was used to compute average jet total pressure. Pressure and temperature measurements in the high pressure plenum were used in the calculation of mass-flow rate. Details for this procedure can be found in reference 30. Forces and moments acting on the metric portion of the model were measured by a six-component strain-gage balance (ref. 30). Static pressure tubes were fixed to the upper external surface of the nozzle model during the entire test program to monitor possible recirculation effects due to the proximity of the reverse thrust exhaust flow to the simulation hardware.

Test Procedure

All of the solid port (nonrotating) configurations were tested over a nozzle pressure ratio range of 1.5 to 6.0. The self-propelled configurations were also tested over a similar nozzle pressure ratio range (up to 5.0). Rotating cylinder port corner configurations were tested over a range of RPM from 0.0 to 10,000 at nozzle pressure ratios of 1.5, 2.0, and 3.0. For all configurations, data were taken in ascending order of nozzle pressure ratio. Rotating cylinder data were taken by setting a constant nozzle pressure ratio and driving the port corner cylinder through the required rotational speed range.

Data Reduction

A data point consisted of 50 samples taken over a time period of approximately 5 seconds. The data were recorded on a magnetic tape using the data acquisition system dedicated to the static test facility. Averaged data were then used in the data reduction process.

The basic parameters used to quantify the internal performance of the 2-D C-D thrust reverser port configuration were resultant gross thrust ratio (F_r/F_i), resultant thrust vector angle (δ), axial thrust ratio (F/F_i), and discharge coefficient (w_p/w_i). Resultant gross thrust ratio (F_r/F_i) is the ratio of measured resultant gross thrust to ideal thrust and is a measure of nozzle internal performance (or efficiency). Resultant gross thrust (F_r) is determined from the corrected axial and normal force thrust components (see Symbols section) which are obtained from strain gage balance measurements. Balance measurements are first corrected for weight tares and balance interactions. More corrections determined for the tests account for the additional jet-off force and moment interactions existing between the bellows flow transfer system (fig. 1) and the force balance. In addition, momentum tare corrections, which result from the imperfect transfer of the high pressure air between the nonmetric and metric portions of the model, are also applied to balance measurements. The procedure for determining these corrections is reported in reference 30. Resultant thrust vector angle (δ) is also calculated using corrected axial and normal force thrust components (see Symbols section) and is measured from the horizontal reference line such that δ = 0 degrees represents cruise or forward thrust nozzle operation. Axial thrust ratio (F/F_i) is a measure of the axial thrust (F) generated as a fraction of the gross thrust (F_i) available. A negative value indicates reverse thrust. Discharge coefficient (w_p/w_i) is the ratio of measured mass-flow rate (w_p) to the ideal mass-flow rate

(w_i) and is a measure of the ability of a nozzle to transfer mass flow. Values of w_p/w_i less than unity result from momentum and vena contracta losses.

CHAPTER III

RESULTS AND DISCUSSION

The basic performance data for each thrust reverser port configuration tested during this investigation are presented in figures 4-8. Discharge coefficient (w_p/w_i), resultant gross thrust ratio (F_r/F_i), axial thrust ratio (F/F_i), and resultant thrust vector angle (δ) are presented as functions of nozzle pressure ratio (NPR) in figures 4, 6, and 8. In figure 5 the same parameters are shown as they vary with port corner cylinder revolutions per minute (RPM). Figure 7 shows the measured variation of port corner cylinder RPM with nozzle pressure ratio (NPR) for four self-propelled, rotating cylinder configurations (confs. 10, and 12-14). As shown in Table I, three additional self-propelled, rotating cylinder configurations (confs. 8, 9, and 11) were tested. However, because of air loads on the cylinders, the port corner cylinders for these configurations did not rotate (RPM = 0.0). Data for these configurations are shown in figure 6 as a function of NPR. These configurations are treated as solid port corner configurations in the remainder of this paper.

Solid Rounded-Corner Port Internal Performance

The port configuration with a solid corner of 0.109 inch radius and located in a constant area duct (conf. 1, see fig. 3(a)) had peak internal performance (F_r/R_i) at an NPR of approximately 2.0 (fig. 4(a)). The fact that peak internal performance occurs at such a low NPR indicates that the port throat is near the port exit and little exhaust flow expansion occurs in the port passage. This characteristic was expected since all port configurations of the current study were designed with a constant area exit passage which should have its throat, under normal circumstances, at the passage exit due to boundary layer build-up along the passage walls. An ideal convergent nozzle

(throat coincident with exit) reaches peak internal performance at a nozzle pressure ratio of 1.89. The short passage length (0.137 inches) also caused poor flow turning ability (less than 120 degrees) at most NPRs as well as low levels of reverse thrust (F/F_i greater than -.50). For typical cruise or forward-thrust mode nozzles, discharge coefficient (w_p/w_i) usually becomes nearly independent of nozzle pressure ratio for NPR greater than 2.0 and attains a value from about 0.96 to 0.99. As shown in figure 4(a), the short passage conf. 1 never becomes independent of NPR (for the range of NPR tested) and only reached a value of 0.883 at NPR = 6.0. These characteristics indicate not only that the port effective throat area (A*) is significantly less than the port geometric throat area (A_t) from which w_i is computed, but also that its magnitude is varying throughout the NPR range tested. The most probable cause of these data trends is exhaust flow separation around the port corner. This separated flow region evidently extends to the port exit since, as discussed previously, the port throat and port exit for this configuration (conf. 1) are nearly coincident. The variation in discharge coefficient is probably caused by a change in the amount of flow separation as NPR is changed. See sketch below.

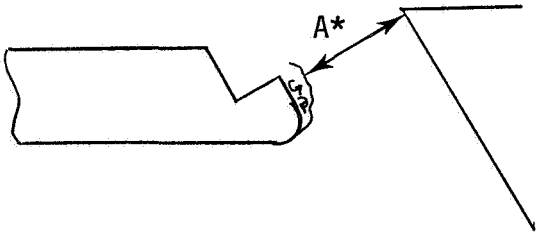

$A^* < A_t$

$A^* \approx A_e$

$\delta < 120$

The port configurations located in a convergent duct (confs. 2 (fig. 4(b)) and 3 (fig. 4(c)) had peak internal performance at nozzle pressure ratios near 4.0. Nozzles which have peak performance at NPR greater than 2.0 generally require some internal expansion in the nozzle (a convergent-divergent nozzle). As previously mentioned, the ports of the current investigation were designed with constant area passages and should exhibit convergent nozzle performance

characteristics. One possible cause for the convergent-divergent nozzle performance characteristics exhibited by the reverser ports located in a convergent duct (confs. 2 and 3) is exhaust flow separation around the port corner and subsequent reattachment to the upstream port wall which would form a separation bubble in the port passage. As indicated in Table I, confs. 2 and 3 had a longer port passage length than conf. 1. An increased passage length could allow exhaust flow reattachment to occur. A separation bubble in the port passage would cause the effective throat area (A*) to be less than the port exit area (A_e) and thus some internal expansion would occur in the port passage. Exhaust flow separation in the port passage would also cause the effective throat area (A*) to be less than the geometric throat area (A_t) and result in low values of discharge coefficient. This result is confirmed by the discharge coefficient data for configurations 2 and 3. The maximum discharge coefficients for the ports located in a convergent duct are significantly lower than for the port configuration located in a constant area duct (conf. 1). The lower discharge coefficients for configurations 2 and 3 are probably caused by more severe port corner flow separation since the exhaust flow must turn through a larger angle to enter the port passage for these configurations (compare geometry of confs. 2 and 3 with conf. 1 in fig. 3). The extent of exhaust flow separation for configurations 2 and 3 apparently stablizes at an NPR of about 3.0 since discharge coefficient is nearly constant for NPR greater than 3.0. The longer passage lengths of these configurations (see fig. 3(a)) provided

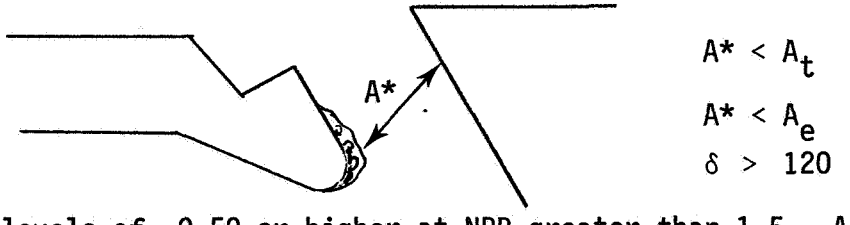

reverse thrust levels of -0.50 or higher at NPR greater than 1.5. A more negative value of F/F_i indicates larger reverse thrust (-F) levels. Because of

the longer passage, the flow turning ability of confs. 2 and 3 exceeded that of the short length passage configuration 1 and also the geometric design angle of 120 degrees. The probable cause for measured resultant thrust vector angles (δ) greater than design is an inclined effective throat area in the passage. An inclined throat would not only tend to turn the flow but also create unequal port wall lengths downstream of the throat and effectively the port would become a single expansion ramp type nozzle. Single expansion ramp nozzles are known to have larger thrust vector angles than design because of unopposed pressures acting on the longer length ramp (refs. 10, 12, 31, and 32). This fact would also explain the larger than design levels of reverse thrust. The increased passage length between configurations 2 and 3 of 0.160 improved the peak internal performance (F_r/F_i) of the port by about 2-percent but had only small effects on the other performance parameters.

The 0.109 inch radius, rotating cylinder port corner configuration (confs. 4-7) at RPM = 0.0 exhibited the same performance trends with NPR as the solid rounded port corners discussed above. As shown in figure 5 rotating the cylinder at RPM up to 10,000 (2.5% of desired RPM, see Appendix) had no effect on F_r/F_i. The variation of F/F_i and resultant thrust vector angle seen at NPR equal to 1.5 is not a real effect of cylinder rotation. The actual corrected force balance variations for the constant NPR fell well within the accuracy of the balance. No effect on reverse thrust ratio or thrust vector angle was noted at NPR greater than 1.5. The effect of cylinder rotation on port discharge coefficient will be discussed in a later section.

Large-Cylinder Port-Corner Internal Performance

The large cylinder port corner performance data presented in figure 6 will be used as the baseline data for comparison with the self-propelled cylinder configurations which rotated. The configurations presented in figure 6 (confs.

8, 9, and 11; see fig. 3(c)) were designed to be self-propelled but during actual test conditions the cylinders did not rotate and these configurations will be considered as solid corner configurations for the remainder of this paper. Since these configurations were designed to have a coincident port throat and port exit (no internal expansion), performance behavior similar to a convergent nozzle was expected. Instead internal performance (F_r/F_i) resembled a convergent-divergent nozzle with peak performance near an NPR of 3.0 (fig. 6). This behavior may be caused by the surface of the cylinder above the port exit acting as an external expansion ramp surface, thus producing internal performance characteristics similar to a single expansion ramp nozzle (refs. 10, 12, 31, 32). Resultant thrust vector angle and axial thrust ratio (reverse thrust) levels fell well below the design values of 120 degrees and -0.5 respectively. Results presented in reference 28 indicate that the effect of blocker angle on reverser port performance is small for a 120 degree port. Based on this result, a comparison of configurations 8, 9, and 11 can be made without consideration of the differences in blocker angles. The only parameter considered for this comparison is the increased length of the downstream port wall (see fig. 3(c)) on configuration 11. Lengthening the aft wall increased thrust vector angle 4 degrees, and increased the level of reverse thrust ratio for all nozzle pressure ratios tested. It should be noted that discharge coefficients for the large cylinder port corner configurations were significantly higher than those presented in figures 4 and 5 for the small radius port corner configurations. The discharge coefficients for the large cylinder port corners approach the lower level of discharge coefficients expected for normal cruise or forward-thrust mode nozzles and indicate reduced flow separation in the port passage.

Two possible causes for the failure of some of the self-propelled configura-

tions (confs. 8, 9, 11) to rotate are proposed. The first problem was a misalignment of some of the model hardware which caused the cylinder to rub against the port corner. The second problem may have been the fin design. The cylinder always reached a static equilibrium with a fin just at the lowest point of the cylinder in the port, thus failing to capture any exhaust flow along the model top wall. To help correct the second problem, troughs with a width equal to fin width were cut into the model top wall at an angle which produced a trough depth of 0.2 inches at the cylinder surface (fin length is also 0.2 inches) as shown in figure 3(c). Configurations 10, and 12-14 were modified in this manner and, as shown in figure 7, autorotation of the self-propelled cylinders did occur, especially for those configurations with cylinders having side located fins (confs. 12-14). Results from reference 29 indicate that exhaust flow along the sides of the duct may be less steady than the flow along the centerline and this may have aided cylinder autorotation. The modified centrally located fin configuration (conf. 10) achieved only very low levels of rotational speed (fig. 7) and the internal performance of this configuration (fig. 8(b)) is nearly identical to that measured for configuration 11 (fig. 6(c)) which did not achieve cylinder autorotation. This result tends to confirm the results of reference 28 which indicated that blocker angle had only small effects on port performance (conf. 10 has a blocker angle of 90 degrees whereas conf. 11 has a blocker angle of 75 degrees). Configuration 13 (fig. 8(c)), the side located fin counterpart of conf. 10, reached cylinder rotational speeds of 40,000 RPM at a nozzle pressure ratio of 3.5 (fig. 7). The effects of port corner cylinder rotation were to decrease resultant gross thrust ratio, and to increase resultant thrust vector angle (compare parts (b) and (c) of fig. 8). A slight increase in discharge coefficient can also be noted for configuration 13 (RPM 40,000) at NPR above 3.0. The reduction in F_r/F_i probably results from

the energy extracted to turn the cylinder. The majority of the energy extraction losses are apparently in the normal thrust component since axial thrust ratio levels are nearly identical to those of conf. 10 (low RPM case). Configurations 12, and 14 had measured cylinder autorotational speeds of 34,000 to 85,000 RPM (fig. 7) at NPR above 2.7. Port corner cylinder rotation increased resultant thrust vector angle slightly but again reduced F_r/F_i (compare confs. 12 and 14 at high RPM with conf. 11 at RPM = 0.0), probably because of energy extracted to turn the cylinder.

Summary of Mass Flow Characteristics

The primary objective of this investigation was to determine the effect of thrust reverser port design and, in particular, the effect of a rotating cylinder at the port corner on the mass-flow characteristics (discharge coefficient) of thrust reverser ports. Summary plots showing the effects of several design parameters, including rotational speed of a cylinder located in the port corner, on discharge coefficient are given in figures 9, and 10. All of the configurations of the current investigation had the same design minimum cross-sectional area or geometric throat area. Table I shows measured or actual throat area (A_t) for each configuration tested. If port throat area, jet total pressure, and jet total temperature are the same for two configurations, then comparison of discharge coefficients is equivalent to a comparison of mass-flow rate since ideal mass-flow rates would be identical. A comparison of mass-flow rates yields important information because jet engines require mass-flow rates within a certain range in order to operate. The F-100 engine used in the F-15 airplane, for example, has an upper tolerance (engine overspeed) corresponding to a 20-percent over area (too much mass-flow) and a lower tolerance (stall margin) corresponding to an 8-percent under area (too little mass flow) (ref. 21). These tolerances are based on an engine operating optimally at a discharge coefficient of

approximately 1.0 (measured mass-flow rate equals the ideal mass-flow rate). Typical cruise or forward-thrust mode nozzles generally have discharge coefficients of 0.96 to 0.99.

The baseline configurations used in the current study for evaluation of the effects on discharge coefficient of rounding the reverser port corner and then replacing the port corner with a rotating cylinder are the sharp corner (radius = 0.0) thrust reversing ports reported in reference 28. These sharp port corner configurations were tested on the same exhaust port model hardware used in the current investigation. A summary of the discharge coefficient data is presented in figure 9 as a function of nozzle pressure ratio. As shown in figure 9, the sharp corner ports of reference 28 have very low port discharge coefficients with the maximum value of 0.78 occurring only at the highest NPR tested with the port located in a constant area duct (fig. 9(a)). Discharge coefficients of this low a magnitude indicate severe exhaust flow separation in the port passage and an effective throat area much smaller than the geometric throat area. Rounding the port corner increased the mass-flow rate (discharge coefficient) of the reverser port significantly, regardless of port passage length or location. Replacing the rounded port corner with a rotating cylinder (RPM = 8000) did not affect mass-flow rate for the range of cylinder RPM tested. The differences in discharge coefficient shown in figures 9(b) and 9(c) between the solid rounded corner and the corner including the cylinder may be the result of deformation of the cylinder towards the port corner during testing changing the shape of the port corner (increasing the entrance to the port passage) and possibly reducing flow separation thus improving discharge coefficient. A comparison of discharge coefficients with rotating self-propelled and nonrotating large cylinders located in the port passage is shown in figure 10. A very small (within data accuracy) increase in discharge coefficient is indicated for the rotating cylinder configuration.

CHAPTER IV

CONCLUSIONS

The effects on port internal performance of rounding and the incorporating a rotating cylinder into several thrust reversing exhaust port corners have been investigated at static conditions. The port configurations were tested at nozzle pressure ratios up to 6.0 in the static test facility of the NASA-Langley 16-Foot Transonic Tunnel. Results of this study indicate the following conclusions:

1. Replacing a sharp corner in the upstream port wall of a reverser with a rounded corner significantly improved discharge coefficient.
2. Incorporating a rotating cylinder into the upstream port wall showed no further improvement in discharge coefficient for the range of cylinder revolutions per minute achieved (surface velocity of cylinder = 2.5% of duct velocity).
3. Reverser ports located in constant area ducts had higher discharge coefficients than reverser ports located in convergent ducts. This probably results from less severe exhaust flow separation around the port corner since total flow turning angle is less for a given design reverser angle.
4. Highest levels of discharge coefficient (approaching cruise or forward mode performance) were obtained with large, rounded cylindrical shaped surfaces in the upstream port wall.

APPENDIX

DISCUSSION OF DRIVEN ROTATING CYLINDER SPEEDS

In an attempt to provide a wide range of RPM to the powered rotating cylinder configurations of the current investigation, two motors were utilized. One was an electric motor with an RPM range of 0 to 10,000 and the other was an air-turbine motor with an RPM range of 10,000 to 100,000. Both motors were regulated from the control room. The maximum desired RPM for each rotating cylinder configuration was chosen as the RPM needed to impart a cylinder surface velocity equal to the local exhaust flow velocity in the duct upstream of the corner. Data for the calculation of surface velocity were obtained from reference 29. For NPR from 2.0 to 5.0 static to total pressure ratios of 0.93 to 0.95 were measured in the duct upstream of the reverser port for a geometrically similar nozzle thrust reverser model. These static pressure ratios correspond to duct velocities on the order of 300-350 ft/s. The required cylinder rotational speeds to obtain this velocity were 400,000 for the small cylinder (0.109 in. radius) and 80,000 for the large cylinder (0.250 in. radius). Calculation of cylinder natural frequencies limited the small cylinder rotation to 130,000 RPM (well below desired RPM) and the large cylinder to 290,000 RPM (well above desired RPM). Within the resources available, the maximum RPM obtainable during this investigation was 100,000 (with the air-turbine motor). Although 100,000 RPM was substantially less than the desired range for small cylinder rotation, it was still somewhat above the desired range for the large cylinder configurations and it was believed that cylinder surface velocity equal to duct exhaust-flow velocity would be achieved with the large cylinder. However, due to small deviations from design, the as-built model had small misalignments between the cylinder and other model hardware. Almost all of the configurations tested required adjustments during model build-up to present the cylinders from binding. Even with careful model buildup, the air-turbine motor still

could not rotate the cylinders. The exhaust flow loads on the rotating cylinder were apparently too great for the air-turbine motor to overcome. Thus all powered rotating cylinder configurations of this investigation utilized only the electric motor to drive the rotating cylinder and the maximum cylinder rotational speed was limited to less than 10,000 RPM (depending on shaft loads which were configuration and NPR dependent). Cylinder rotational speeds of 10,000 RPM were well below the desired maximum RPM (surface velocity) for both cylinder sizes and may account for the general overall insensitivity of port internal performance to cylinder rotation. It should be noted that for a full-scale application to this concept, the required maximum cylinder RPM (to match exhaust flow velocity) would be significantly less than was required for the subscale model used in this investigation. For a given surface exhaust flow velocity (which is independent of hardware scale), required RPM is inversely proportional to rotating cylinder radius.

REFERENCES

1. Brown, H.; and Fisk, W. S.: Integrated Flight and Propulsion Operating Modes for Advanced Fighter Engines. ASME Paper No. 83 6T 194, March 1983.

2. Lind, G. W.; and Tampler, G.: V/STOL Technology Requirements for Future Fighter Aircraft. AIAA Paper No. 81-1360, July 1981.

3. May, R. J.; and Richey, G. K.: Propulsion System and Airframe Integration Consideration for Advanced Air-to-Surface Aircraft. AIAA Paper No. 79-1120, June 1979.

4. Bowers, D. L.; and Laughrey, J. A.: Integration of Advanced Exhaust Nozzles. AGARD Conference Proceedings, No. 301 (Aerodynamics of Power-Plant Installation), September, 1981.

5. Pendergraft, O. C., Jr.: Comparison of Axisymmetric and Non-axisymmetric Nozzles Installed on the F-15 Configuration. AIAA Paper No. 77-842, July 1977.

6. Schnell, W. C.; Grossman, R. L.; and Hoff, G. E.: Comparison of Nonaxisymmetric and Axisymmetric Nozzles Installed on a V/STOL Fighter Model. SAE Paper No. 770983, November 1977.

7. Hiley, P. E.; Kitzmiller, D. E.; and Willard, C. M.: Installed Performance of Vectoring/Reversing Nonaxisymmetric Nozzles. AIAA Paper No. 77-1022, July 1978.

8. Hinz, W.; and Miller, E. H.: Propulsion Integration of a Supersonic Cruise Strike Fighter. AIAA Paper No. 79-0100, January 1979.

9. Miller, E. H.; and Protopapas, J.: Nozzle Design and Integration in an Advanced Supersonic Fighter. AIAA Paper No. 79-1813, August 1979.

10. Capone, F. J.; and Berrier, B. L.: Investigation of Axisymmetric Nozzles Installed on a 0.10-Scale F-18 Prototype Airplane Model. NASA TP 1638, 1980.

11. Glidewell, R. J.: and Warburton, R. E.: Advanced Exhaust Nozzle Technology. AGARD Conference Proceedings No. 301, September 1981.

12. Capone, F. J.: Aeropropulsive Characteristics at Mach Numbers up to 2.2 of Axisymmetric and Nonaxisymmetric Nozzles Installed in an F-18 Model. NASA TP 2044, 1982.

13. Capone, F. J.; and Reubush, D. E.: Effects of Varying Podded Nacelle-Nozzle Installations on Transonic Aeropropulsive Characteristics of a Supersonic Fighter Aircraft. NASA TP 2120, 1983.

14. Carson, G. T., Jr.; Capone, F. J.; and Mason, M. L.: Aeropropulsive Characteristics of Nonaxisymmetric Nozzle Thrust Reversers at Mach Numbers from 0.0 to 1.20. NASA TP 2306, 1983.

15. Willard, C. M.; Capone, F. J.; Konarsky, M.; and Stevens, H. L.: Static Performance of Vectoring/Reversing Nonaxisymmetric Nozzles. AIAA Paper No. 77-840, July 1977.

16. Capone, F. J.: Static Performance of Five Twin-Engine Nonaxisymmetric Nozzles with Vectoring and Reversing Capability. NASA TP 1224, 1978.

17. Berrier, B. L.; and Re, R. J.: Effect of Several Geometric Parameters on the Static Internal Performance of Three Nonaxisymmetric Nozzle Concepts. NASA TP 1468, 1979.

18. McLafferty, G. H.; and Peterson, J. L.: Results of Tests of a Rectangular Vectoring/Reversing Nozzle on an F-100 Engine. AIAA Paper No. 83-1285, June 1983.

19. Re, R. J.; and Leavitt, L. D.: Static Internal Performance Including Thrust Vectoring and Reversing of Two-Dimensional Convergent-Divergent Nozzles, NASA TP 2253, 1984.

20. Hakim, A.; Arena, A. V.; and Obye, R. C.: Axisymmetric Approach and Landing Thrust Reverser Concepts: Static Performance Results. AIAA Paper No. 83-1227, June 1983.

21. Leavitt, L. D.; and Re, R. J.: Static Internal Performance Characteristics of Two Thrust Reverser Concepts for Axisymmetric Nozzles. NASA TP 2025, 1982.

22. Hiley, P. E.; and Bowers, D. L.: Advanced Nozzle Integration for Supersonic Strike Fighter Application. AIAA Paper No. 81-1441, July 1981.

23. Stevens, H. L.; Thayer, E. B.; and Fullerton, J. F.: Development of the Multi-Function 2-D/C-D Nozzle. AIAA Paper No. 81-1491, July 1981.

24. Dusa, D. J.; Speir, D. W.; and Dunbar, D. K.: Multi-Functional Nozzle for Advanced Weapon Systems. SAE Paper 831426, October 1983. (Published in Proceedings of the Aerospace Congress and Exposition, Oct. 1983, pp. 9-19.)

25. Capone, F. J.: The Nonaxisymmetric Nozzle - It is for Real. AIAA Paper No. 79-1810, August 1979.

26. Laughrey, J. A.; Drape, D. J.; and Hiley, P. E.: Performance Evaluation of an Air Vehicle Utilizing Nonaxisymmetric Nozzles. AIAA Paper No. 79-1811, August 1979.

27. Dusa, D. J.; Speir, D. W.; Rowe, R. K.; and Leavitt, L. D.: Advanced Technology Exhaust Nozzle Development. AIAA Paper No. 83-1286, June 1983.

28. Re, R. J.; and Mason, M. L.: Port Geometry Effects on Thrust Reverser Static Performance. AIAA Paper No. 85-1345, July 1985.

29. Putnam, L. E.; and Strong, E. B.: Internal Pressure Distribution for a Two-Dimensional Thrust-Reversing Nozzle Operating at a Free-Stream Mach Number of Zero. NASA TM 85655, 1983.

30. Peddrew, K. H., compiler: A User's Guide to the Langley 16-Foot Transonic Tunnel. NASA TM 83186, 1981.

31. Re, R. J.; and Berrier, B. L.: Static Internal Performance of Single Expansion Ramp Nozzles with Thrust Vectoring and Reversing. NASA TP 1962, 1982.

32. Berrier, B. L.; and Leavitt, L. D.: Static Internal Performance of Single-Expansion-Ramp Nozzles with Thrust-Vectoring Capability up to 60°. NASA TP 2364, 1984.

TABLE I

SUMMARY OF PORT CORNER DETAILS

conf.	port corner radius	type of duct	cylinder location	fin location	cylinder rotation	A_t (in^2)	constant area port length (in)	exit wall length (in)	β (degrees)
1	0.109	constant area	none	none	none	2.61	0.137	0.231	120
2	↓	convergent	↓	↓	↓	2.62	0.491	↓	↓
3	↓	↓	↓	↓	↓	2.63	0.671	0.400	↓
4	↓	constant area	port corner	↓	CCW	2.61	0.137	0.231	↓
5	↓	convergent	↓	↓	↓	2.58	0.491	0.231	↓
6	↓	↓	↓	↓	CW	↓	↓	↓	↓
7	↓	↓	↓	↓	CCW	↓	0.651	0.400	↓
8	0.250	constant area	↓	center	none	2.64	0.000	0.231	↓
9	↓	↓	↓	↓	↓	↓	↓	↓	90
10	↓	↓	↓	↓	CCW	↓	↓	0.340	↓
11	↓	↓	↓	↓	none	↓	↓	↓	75
12	↓	↓	↓	side	CCW	2.63	↓	↓	120
13	↓	↓	↓	↓	↓	↓	↓	↓	90
14	↓	↓	↓	↓	↓	↓	↓	↓	75
ref. 28 # 1	0.000	↓	none	none	none	2.59	0.491	0.400	120
ref. 28 # 2	↓	convergent	↓	↓	↓	↓	↓	0.231	↓

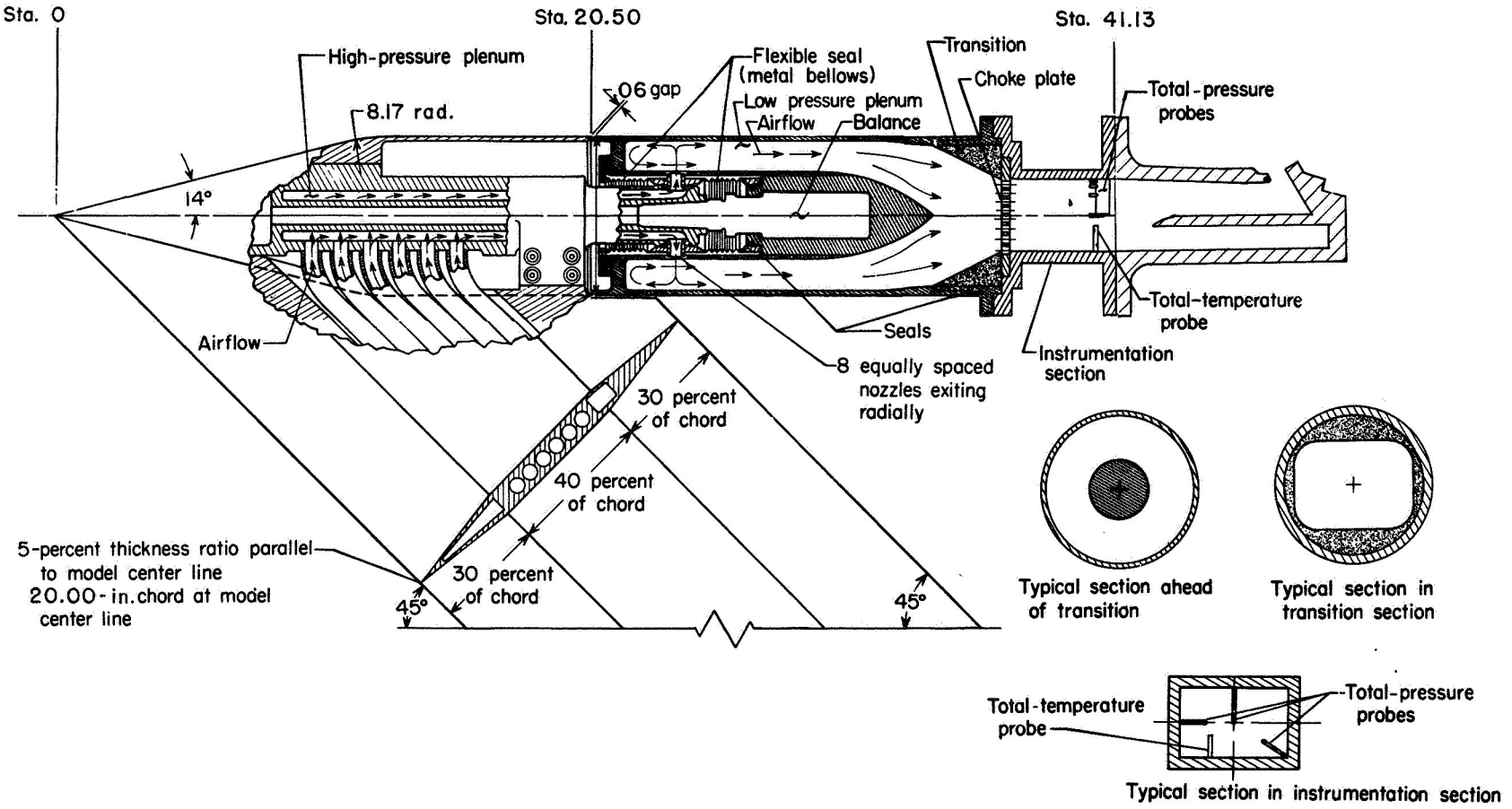

Figure 1. Sketch of air powered nacelle with typical nozzle model installed. All dimensions in inches except as noted.

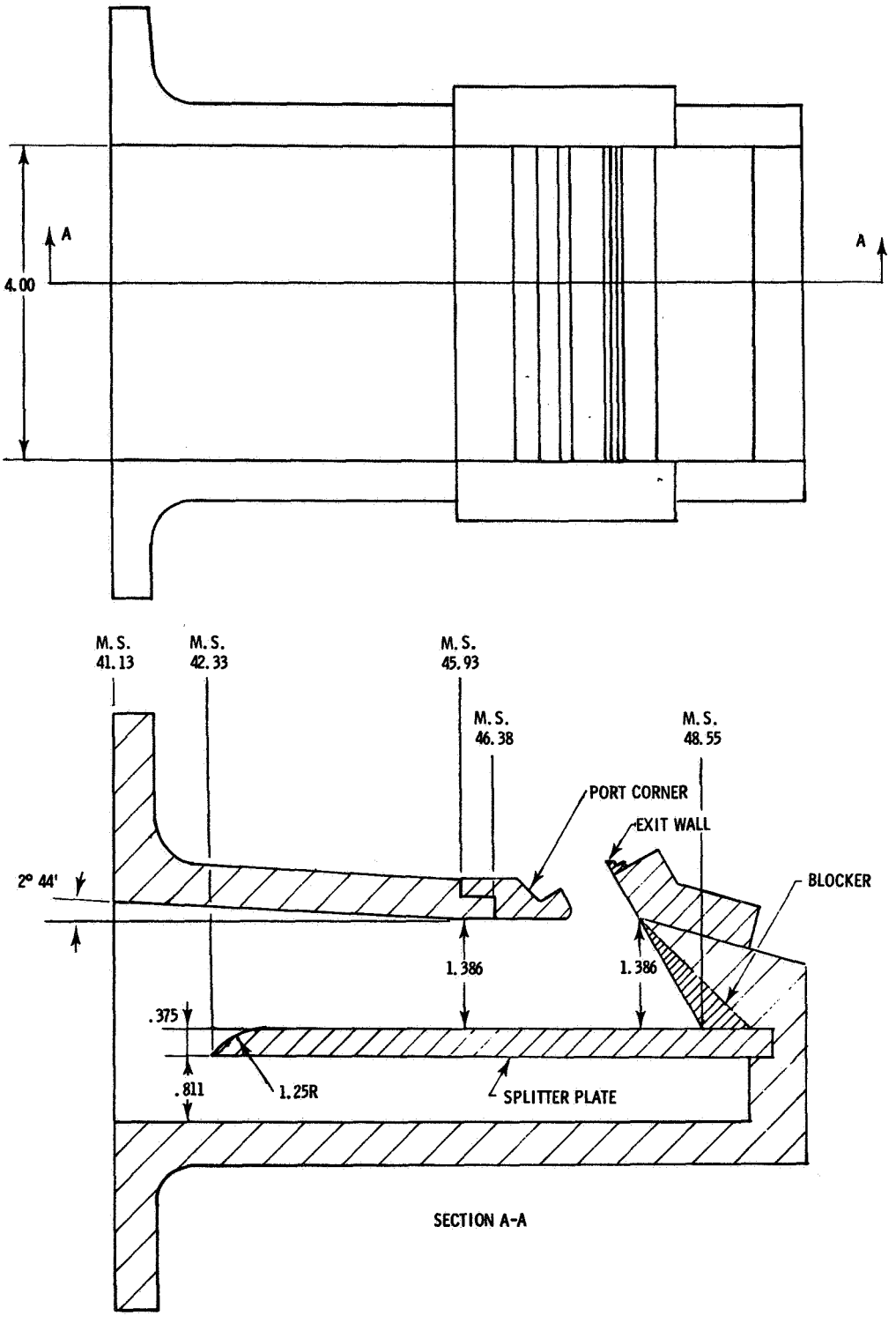

(a) Typical solid rounded corner configuration.

Figure 2. Sketch of thrust reverser exhaust ports. All dimenions in inches except as noted.

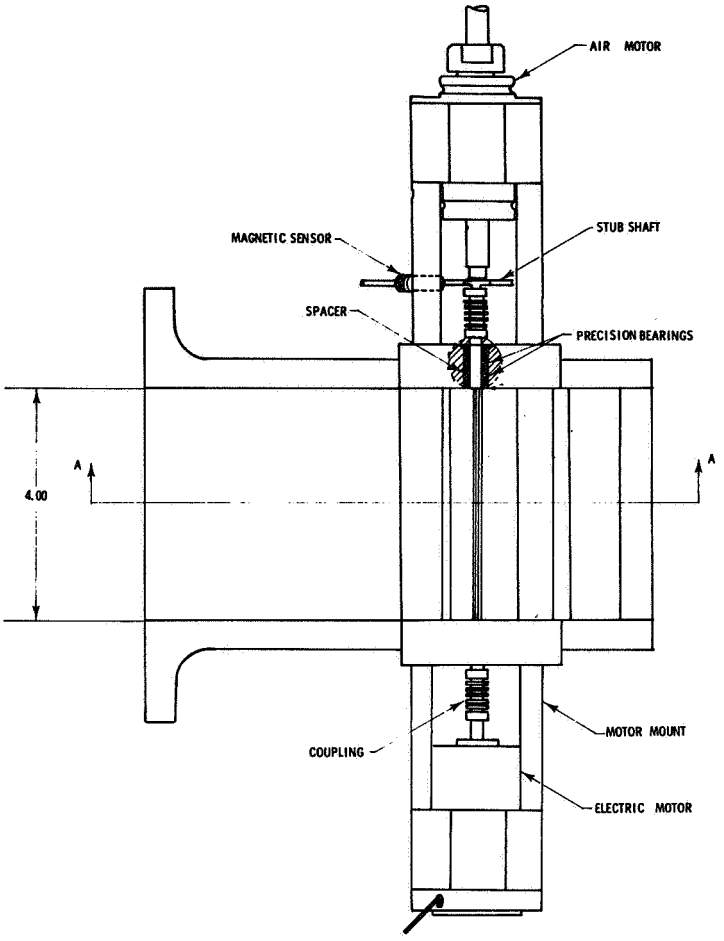

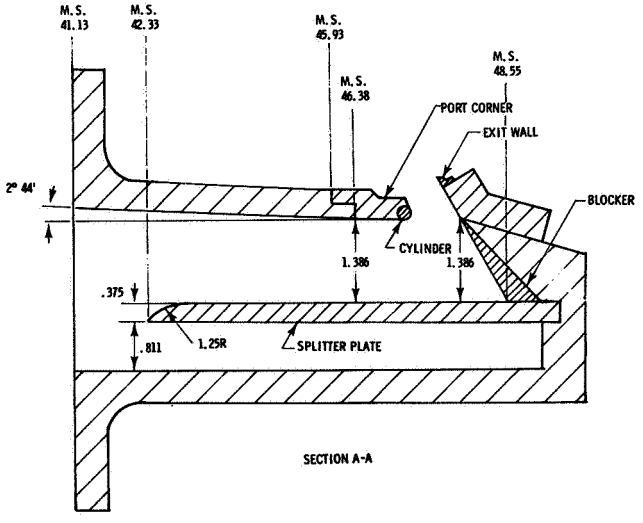

(b) Typical rotating cylinder port corner configuration.

Figure 2. Continued.

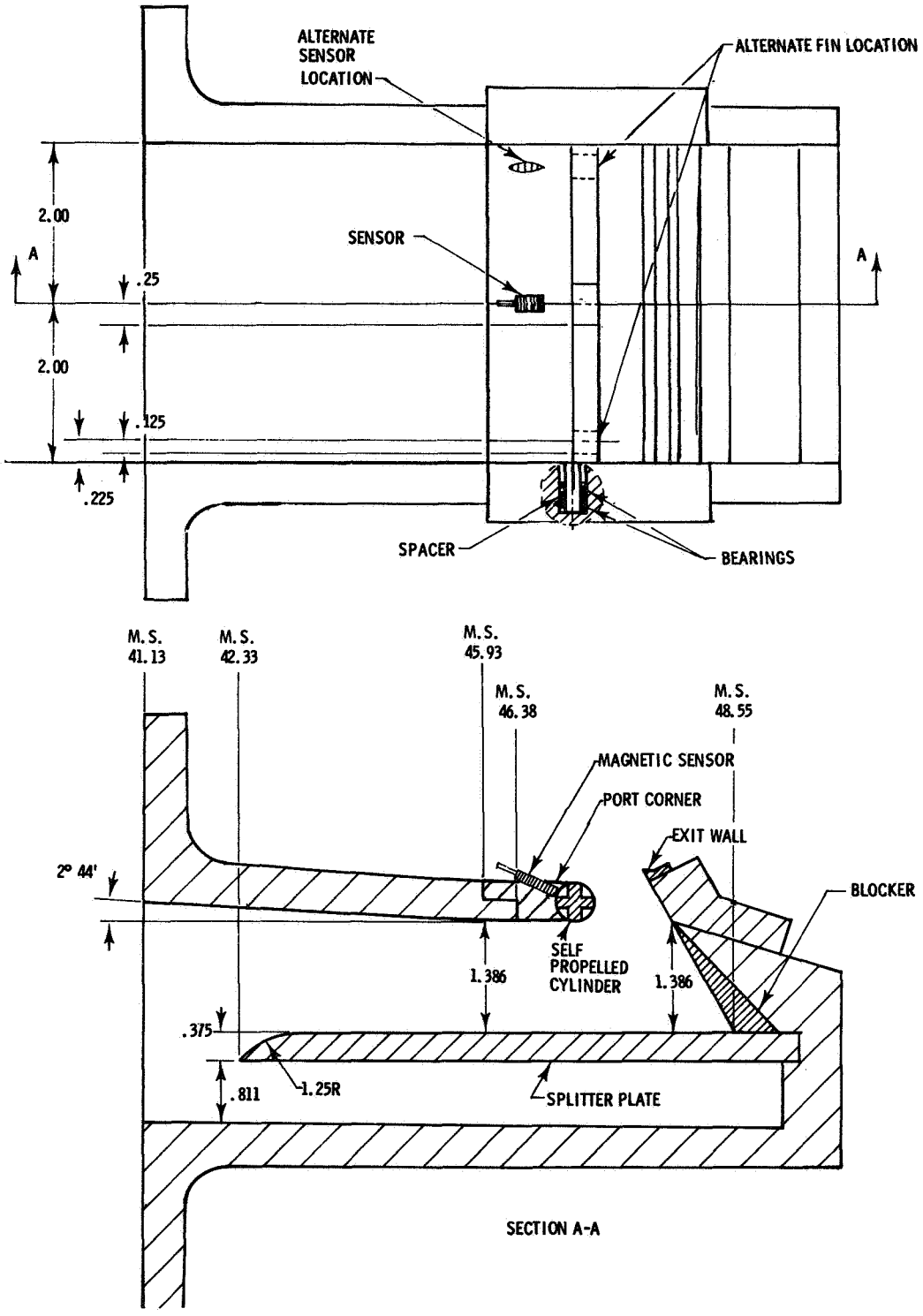

(c) Typical self-propelled rotating cylinder port corner configuration.

Figure 2. Concluded.

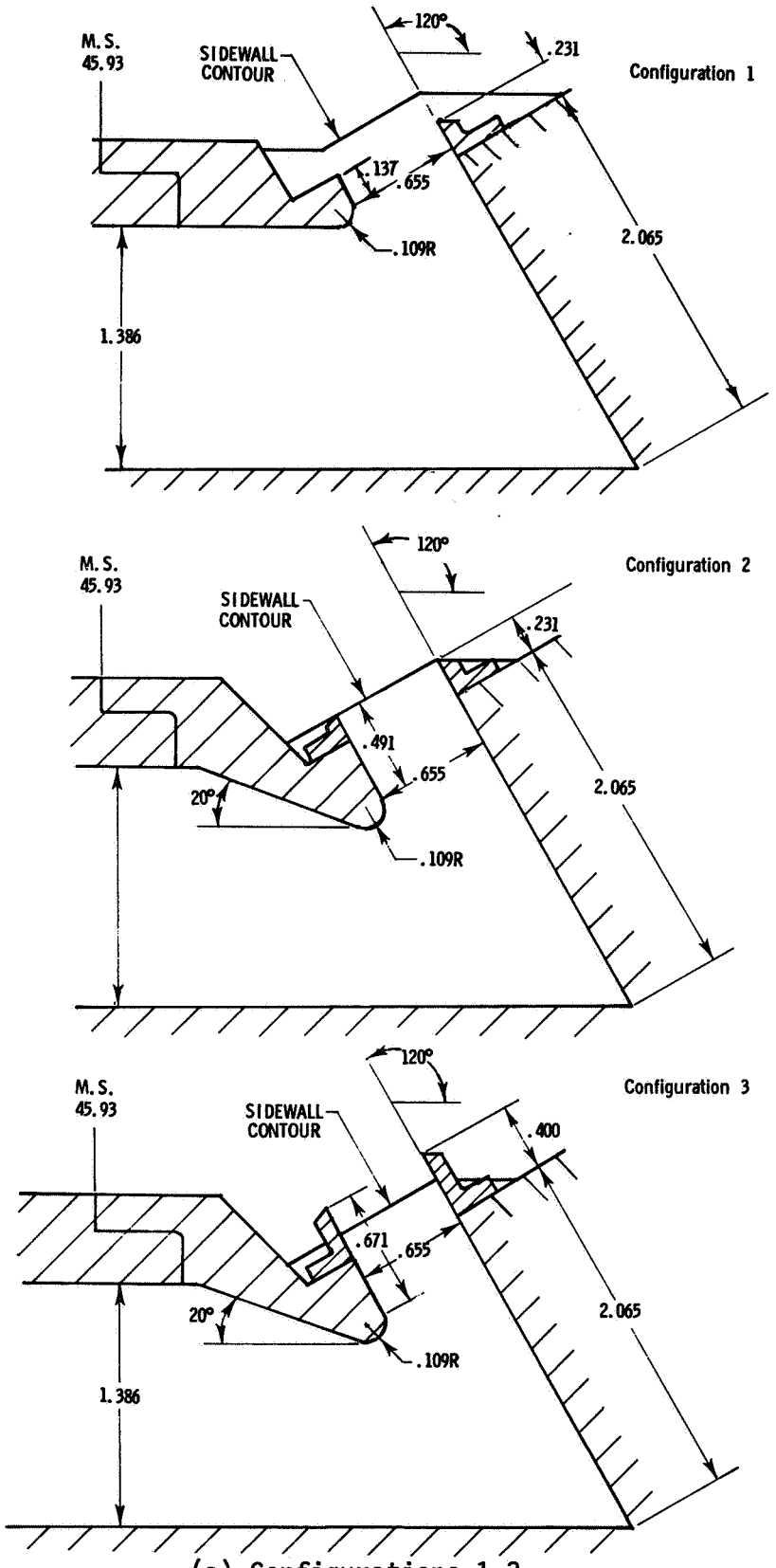

(a) Configurations 1-3.

Figure 3. Sketches of thrust reversing port details. All dimensions in inches except as noted.

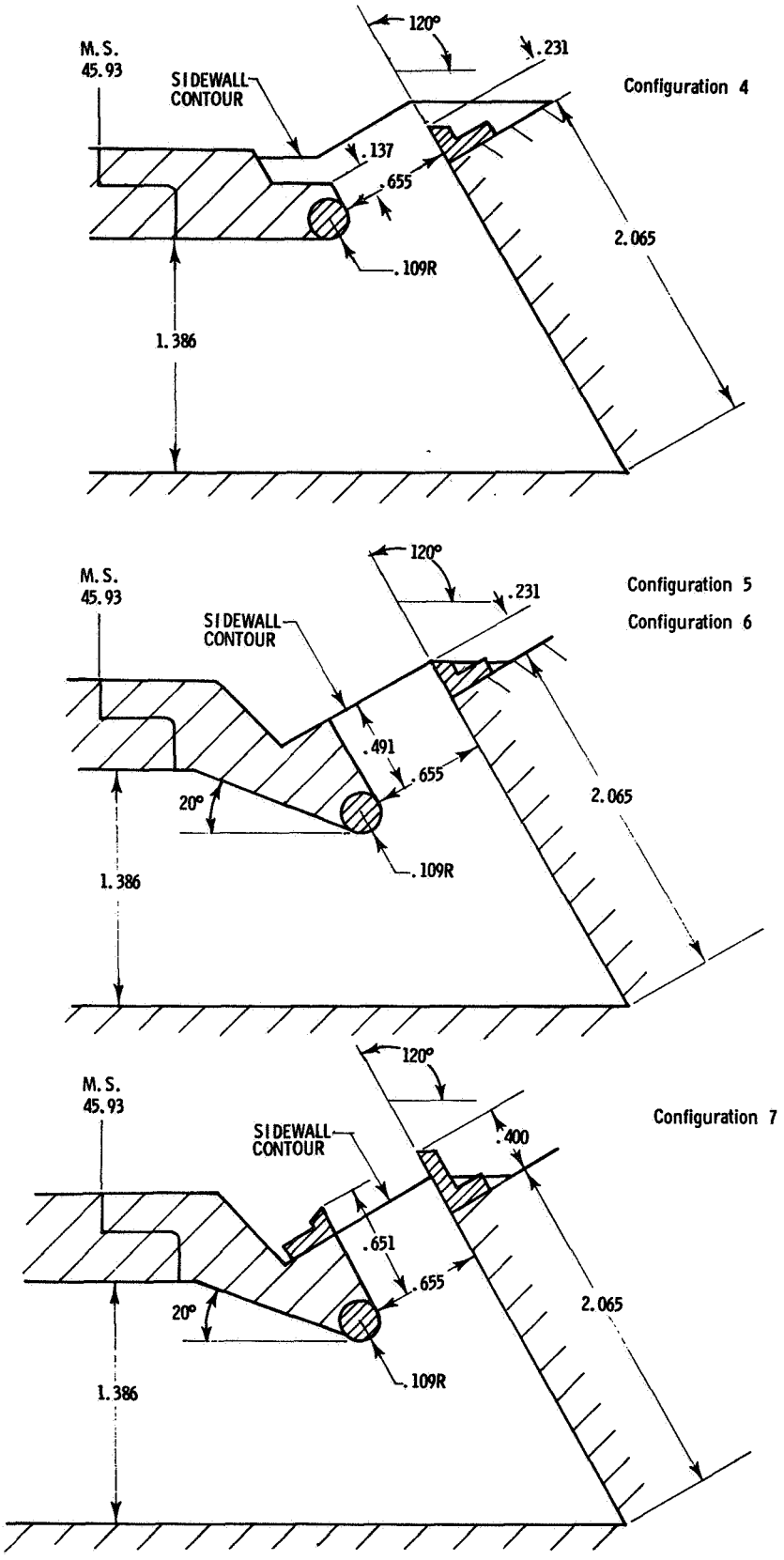

(b) Configurations 4-7.

Figure 3. Continued.

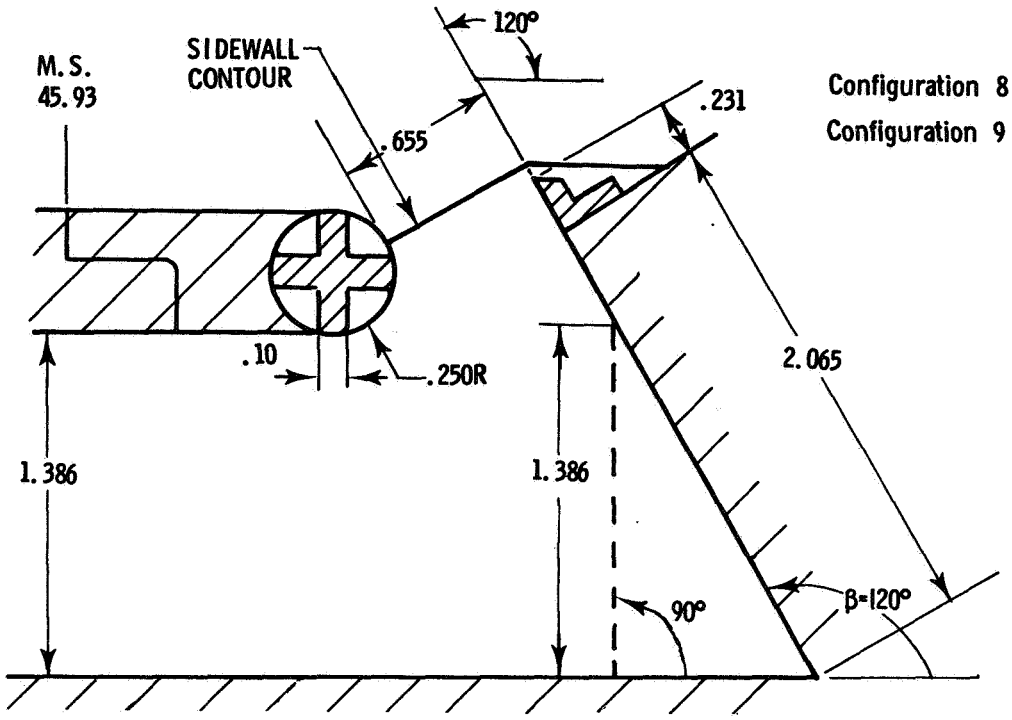

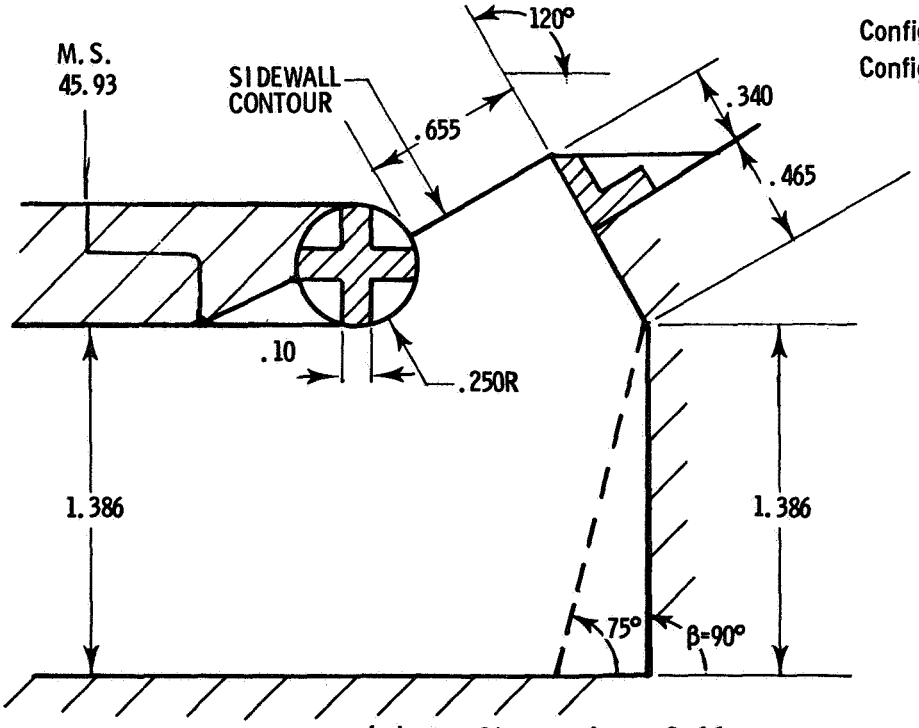

(c) Configurations 8-11.

Figure 3. Continued.

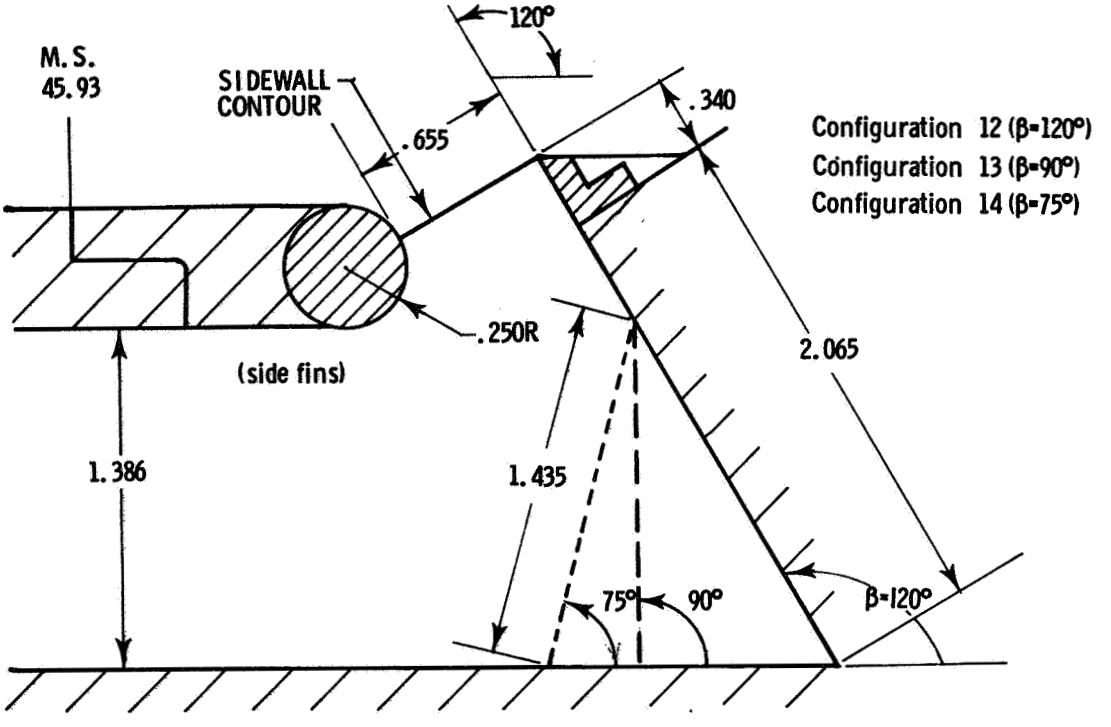

(d) Configurations 12-14.

Figure 3. Concluded.

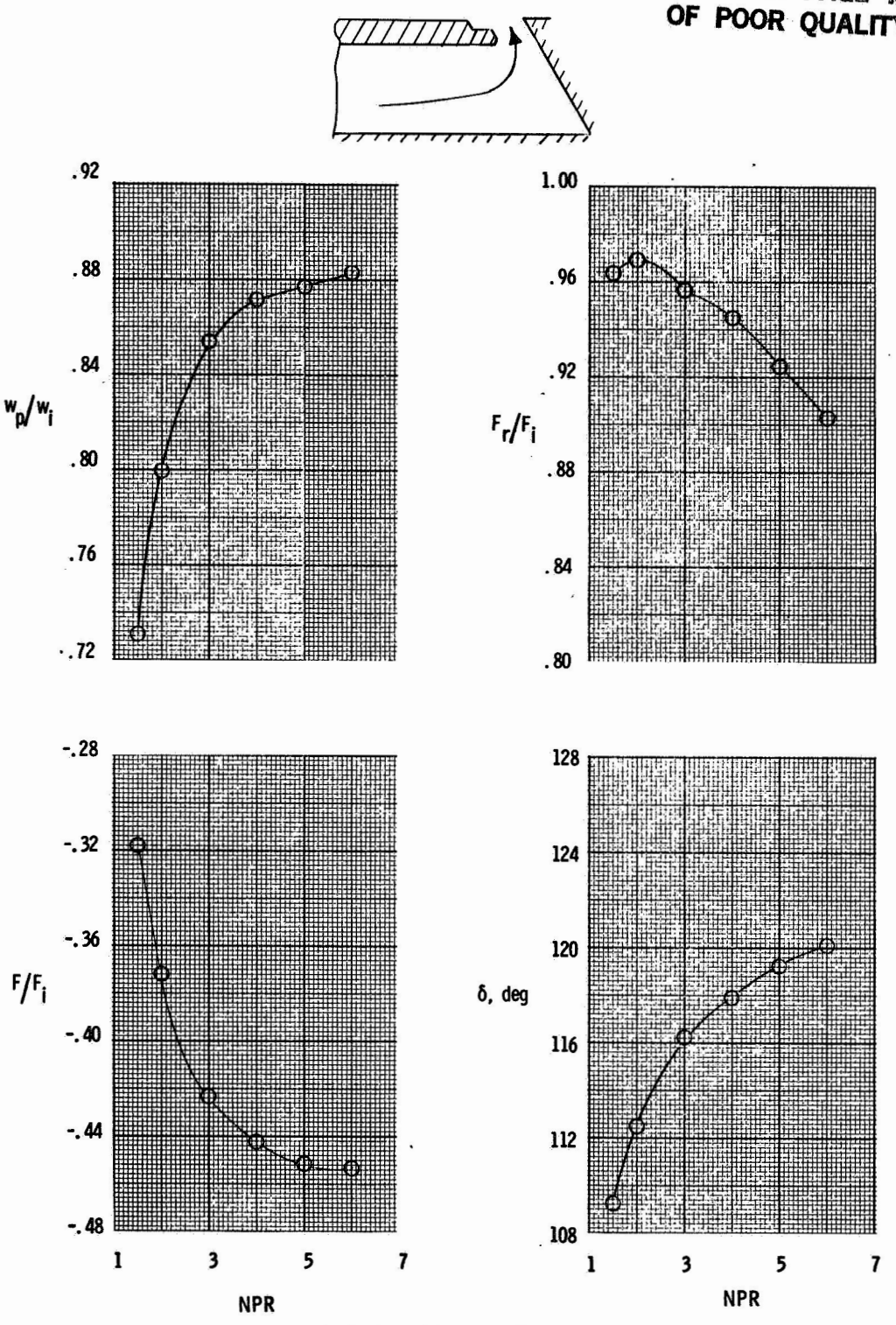

(a) Configuration 1.

Figure 4. Variation of discharge coefficient(w_p/w_i), resultant gross thrust ratio(F_r/F_i), axial thrust ratio(F/F_i), and thrust vector angle(δ) with nozzle pressure ratio(NPR).

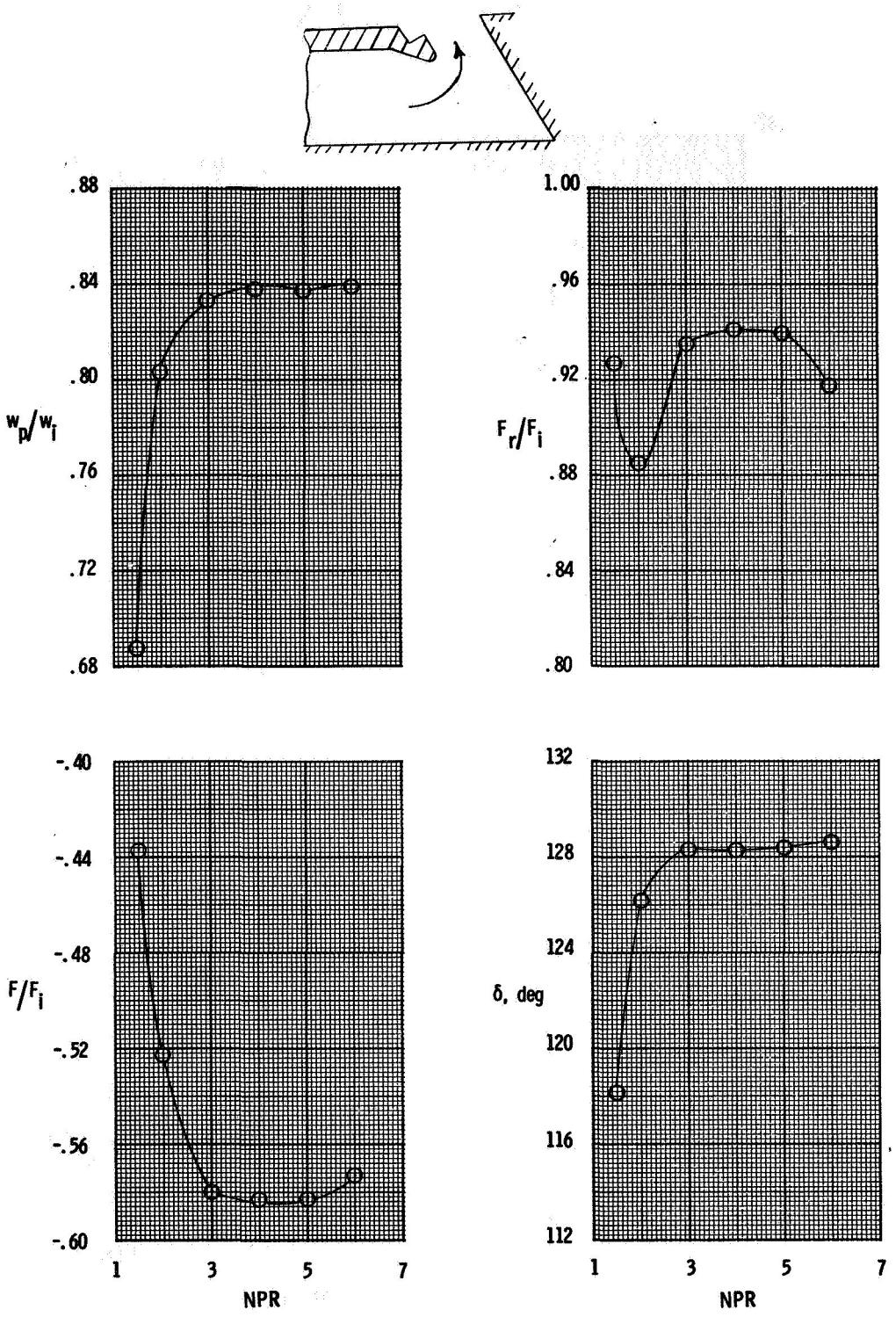

(b) Configuration 2.

Figure 4. Continued.

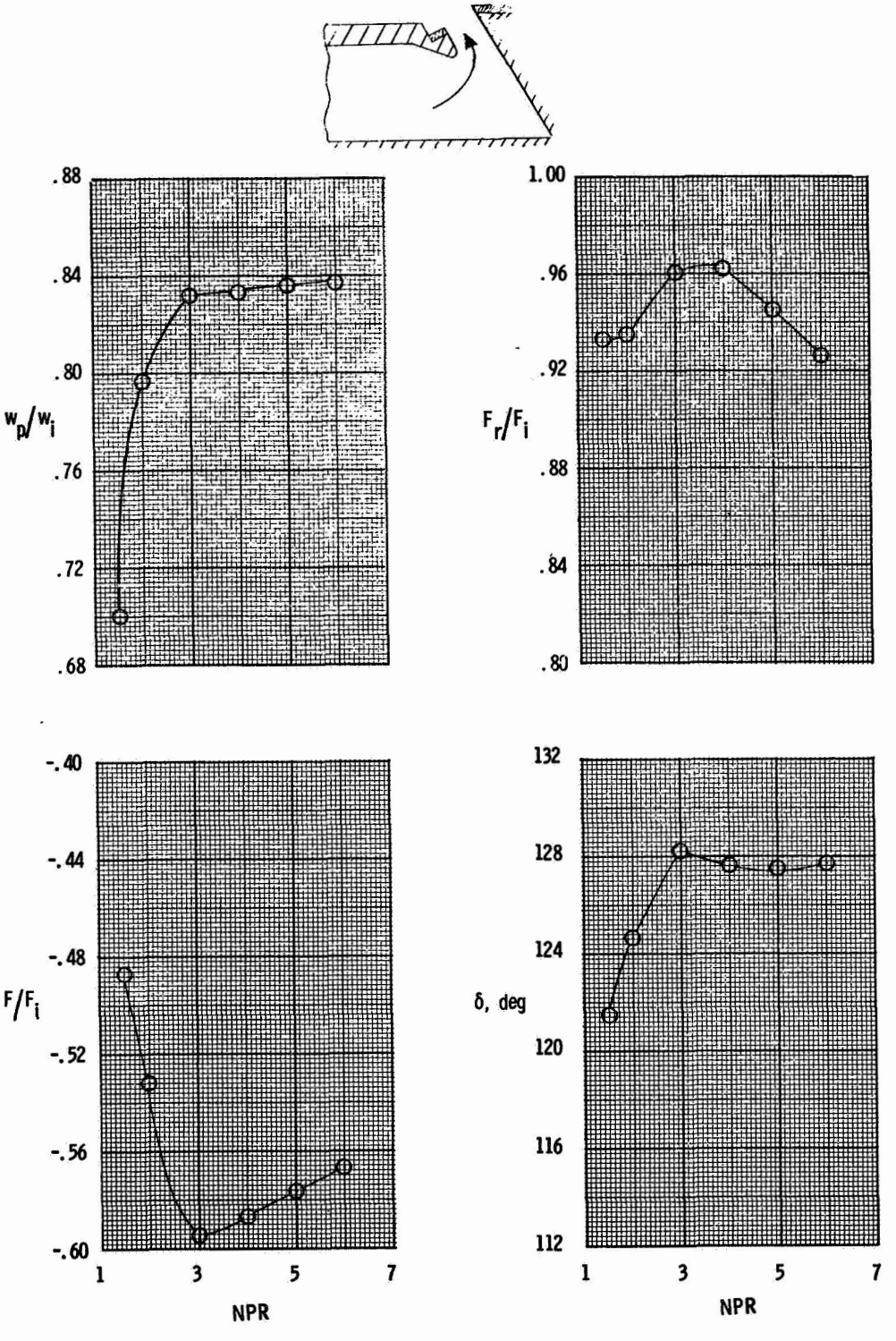

(c) Configuration 3.

Figure 4. Concluded.

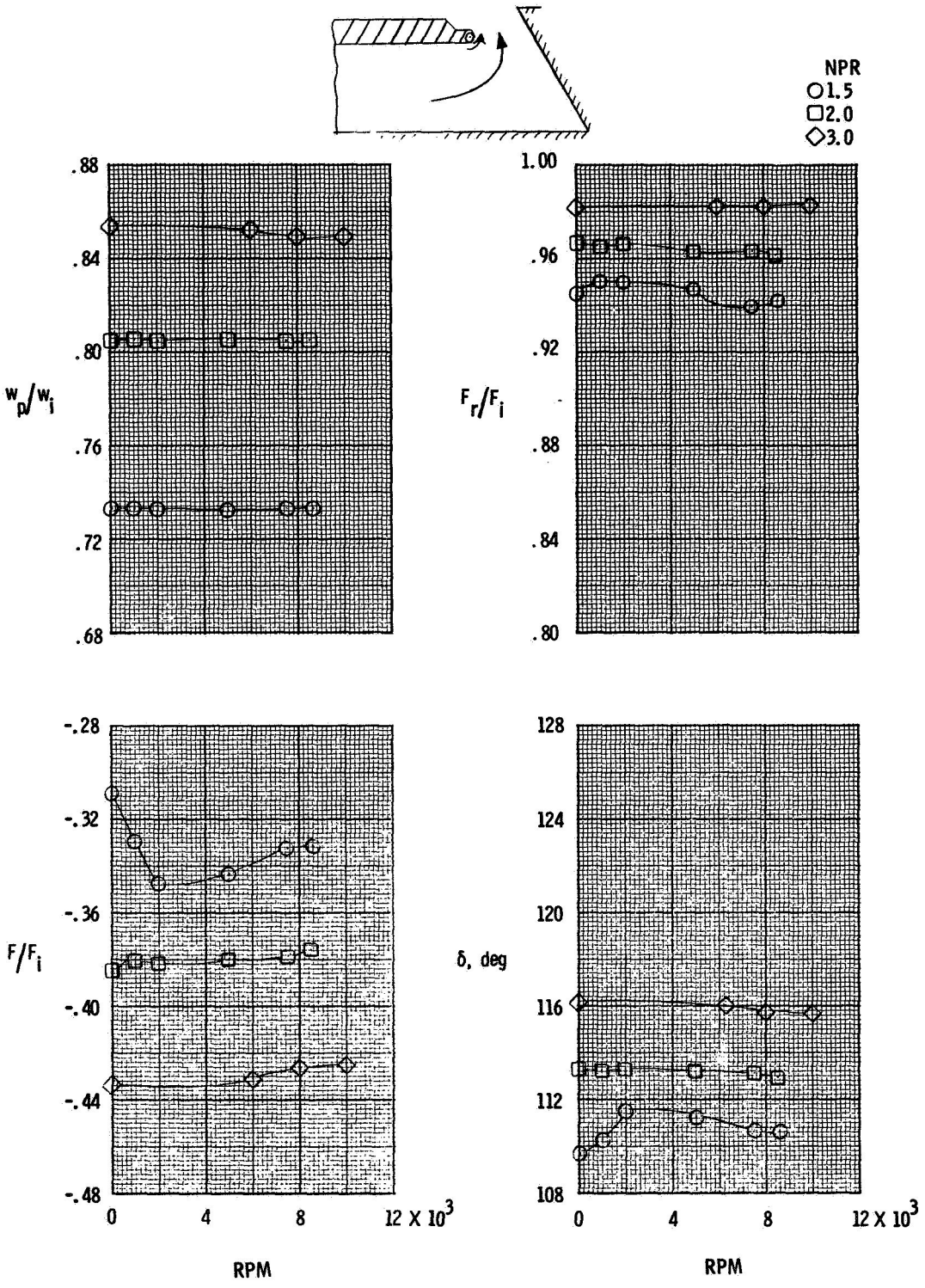

(a) Configuration 4.

Figure 5. Variation of discharge coefficient(w_p/w_i), resultant gross thrust ratio(F_r/F_i), axial thrust ratio(F/F_i), and thrust vector angle(δ) with cylinder revolutions per minute(RPM) for 0.109 inch radius cylinder configurations.

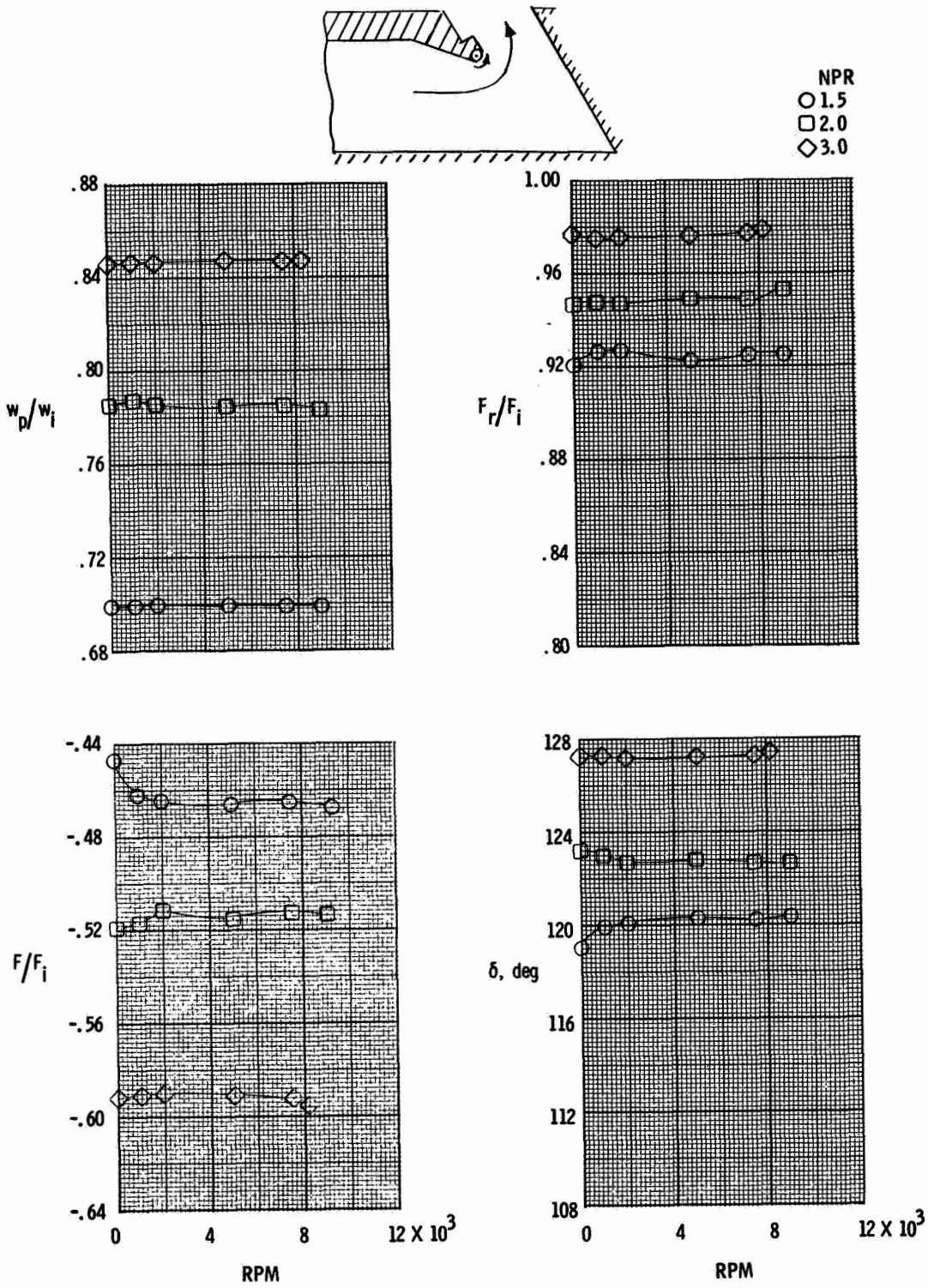

(b) Configuration 5.

Figure 5. Continued.

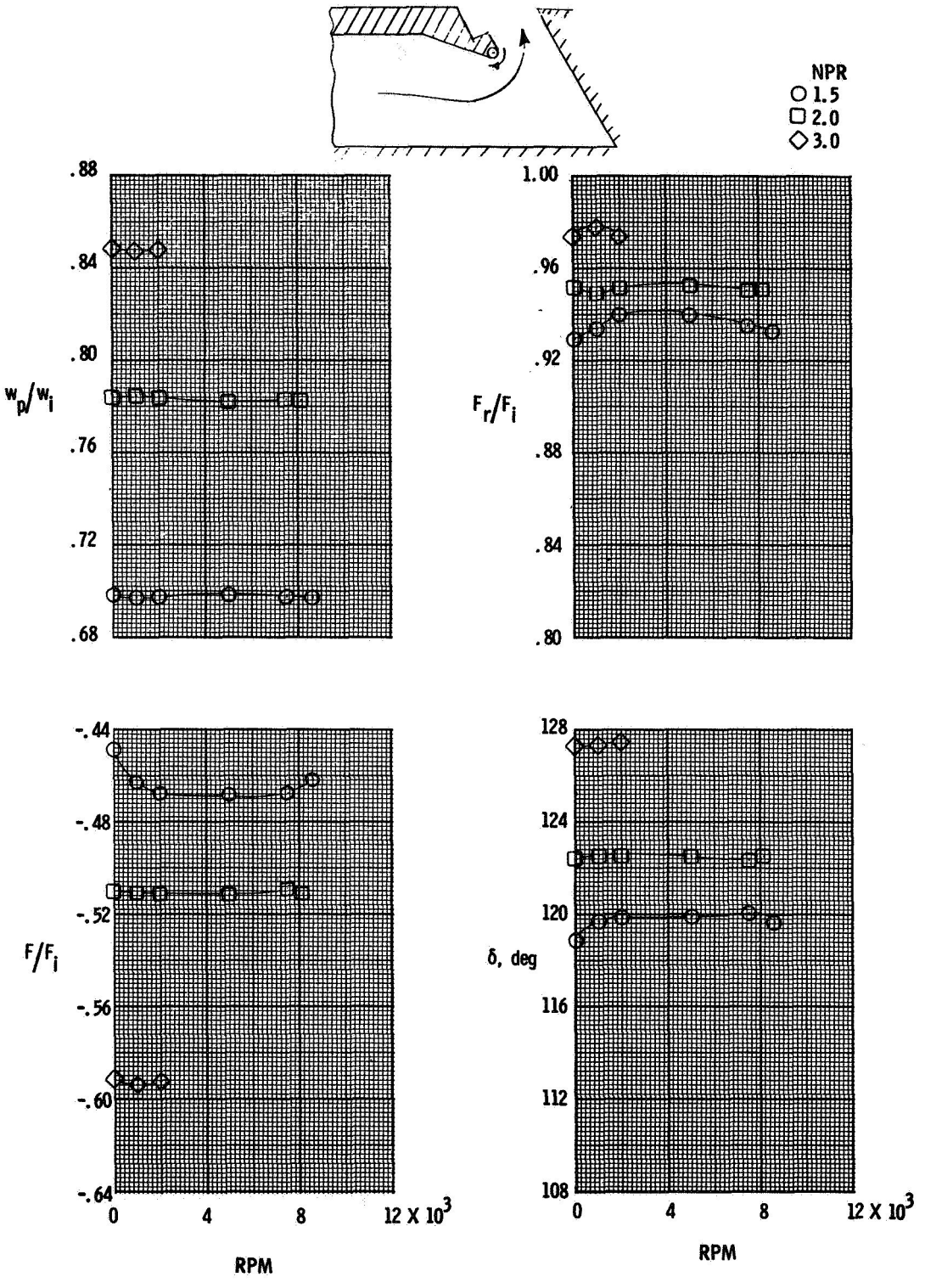

(c) Configuration 6.

Figure 5. Continued.

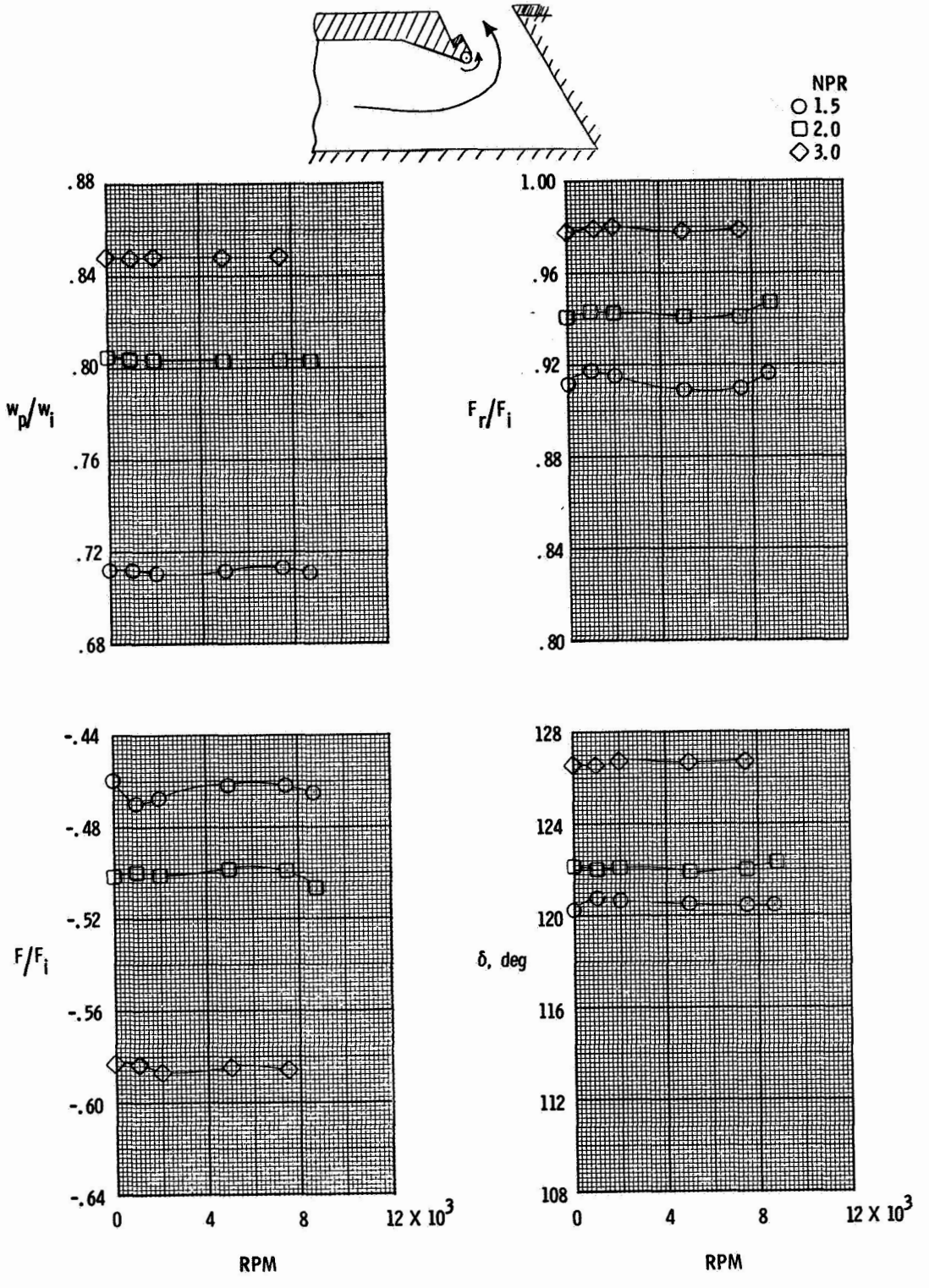

(d) Configuration 7.

Figure 5. Concluded.

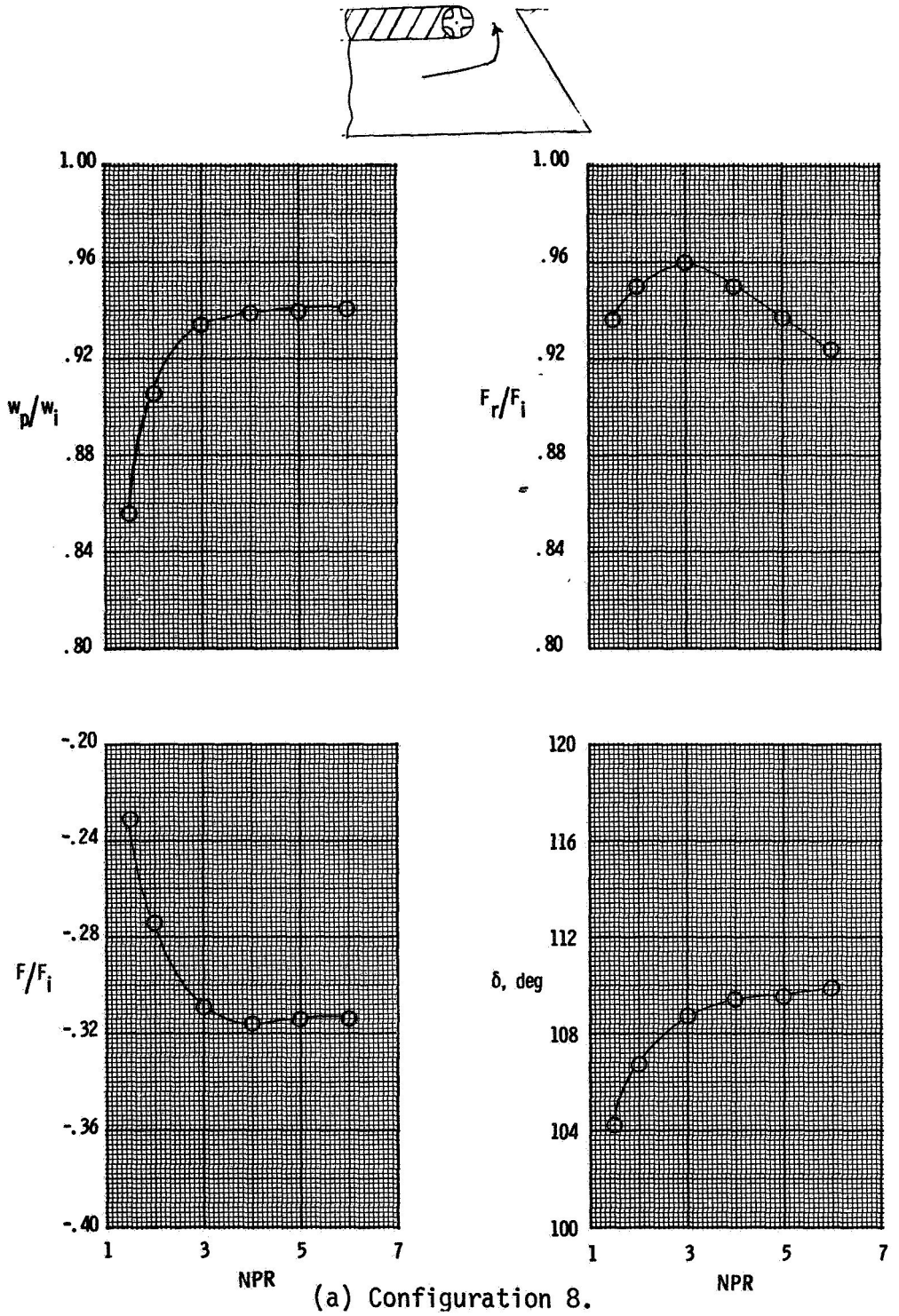

(a) Configuration 8.

Figure 6. Variation of discharge coefficient(w_p/w_i), resultant gross thrust ratio(F_r/F_i), axial thrust ratio(F/F_i), and thrust vector angle(δ) with nozzle pressure ratio(NPR) for 0.250 inch radius self-propelled cylinder configurations at RPM = 0.0.

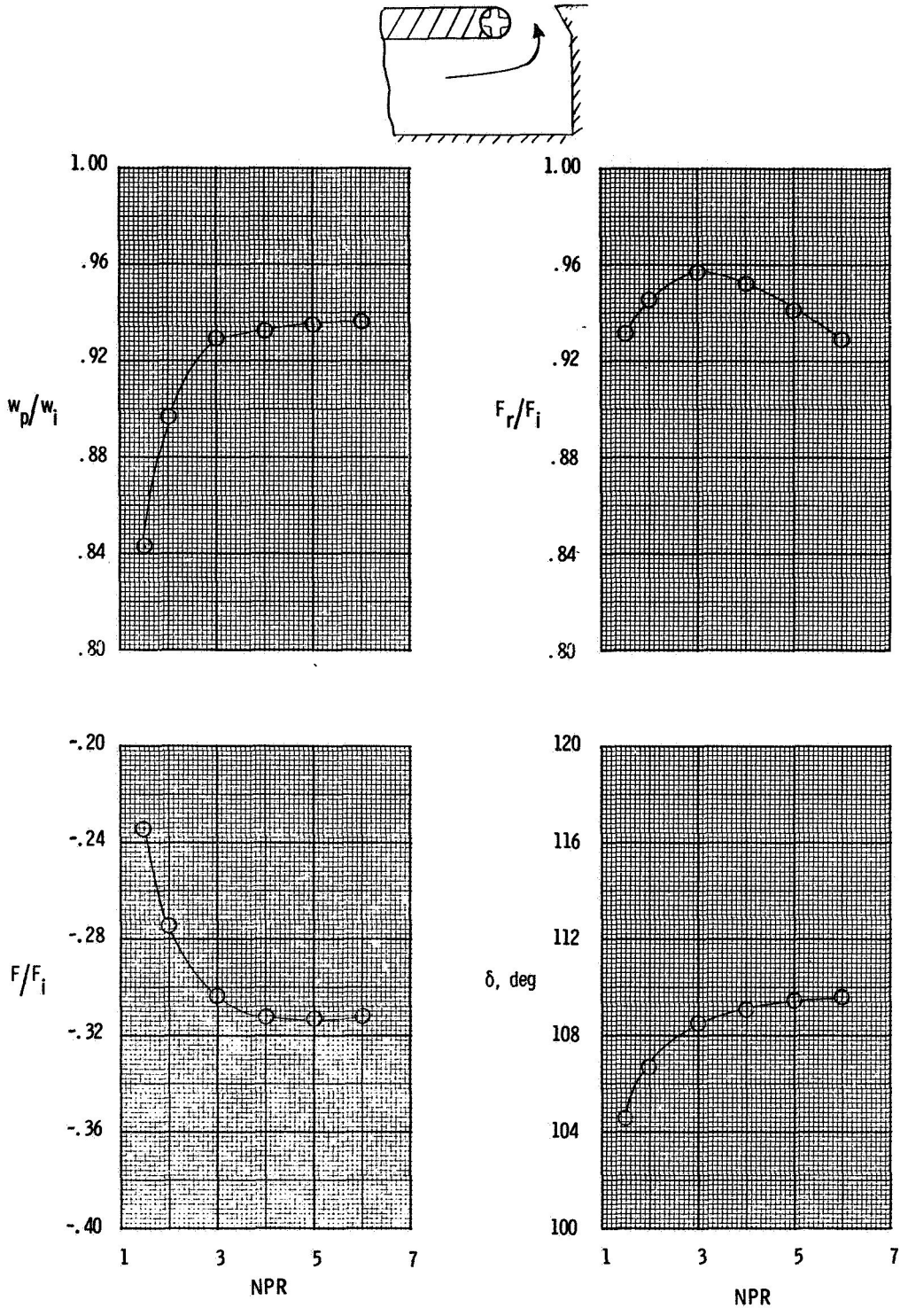

(b) Configuration 9.

Figure 6. Continued.

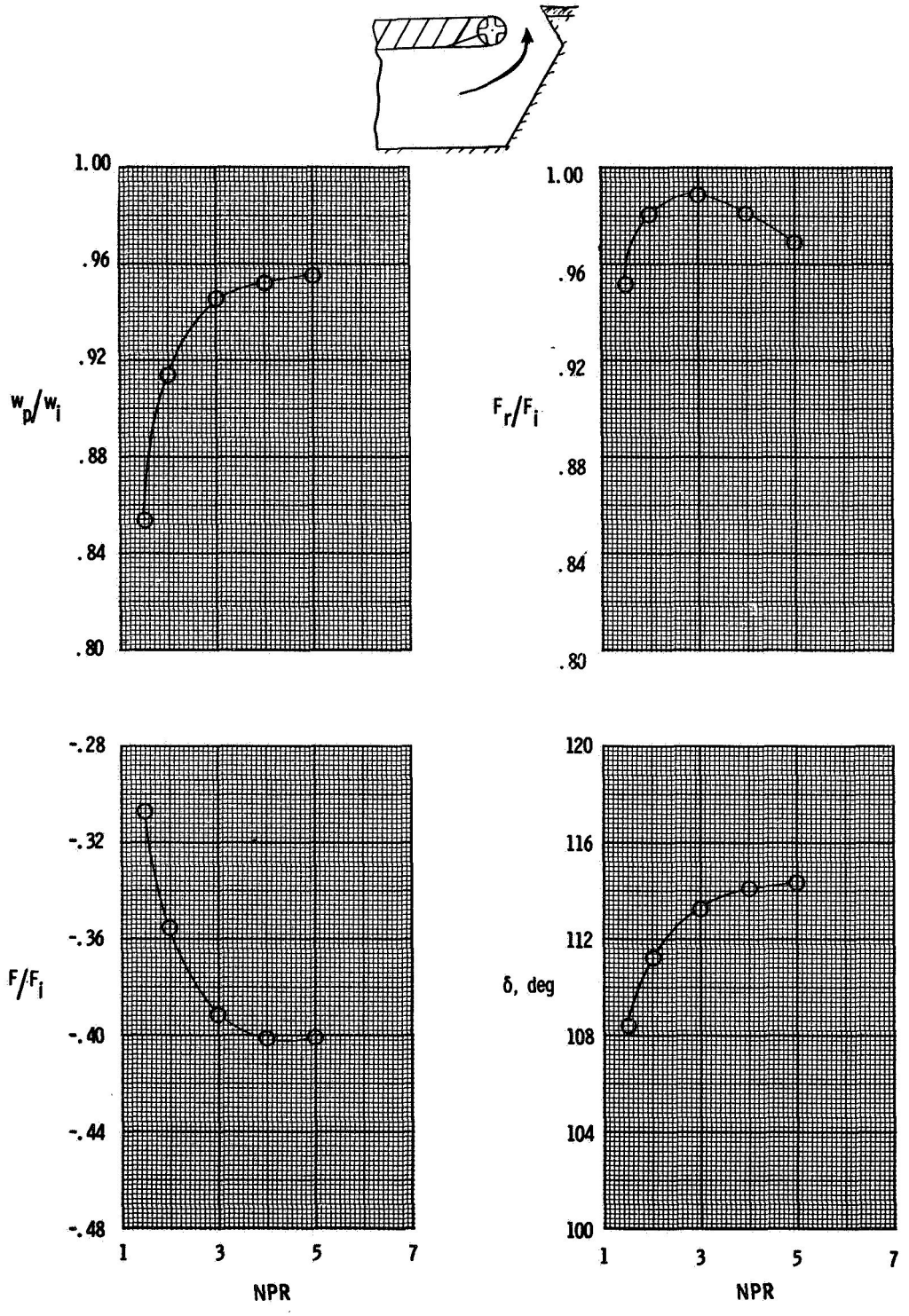

(c) Configuration 11.

Figure 6. Concluded.

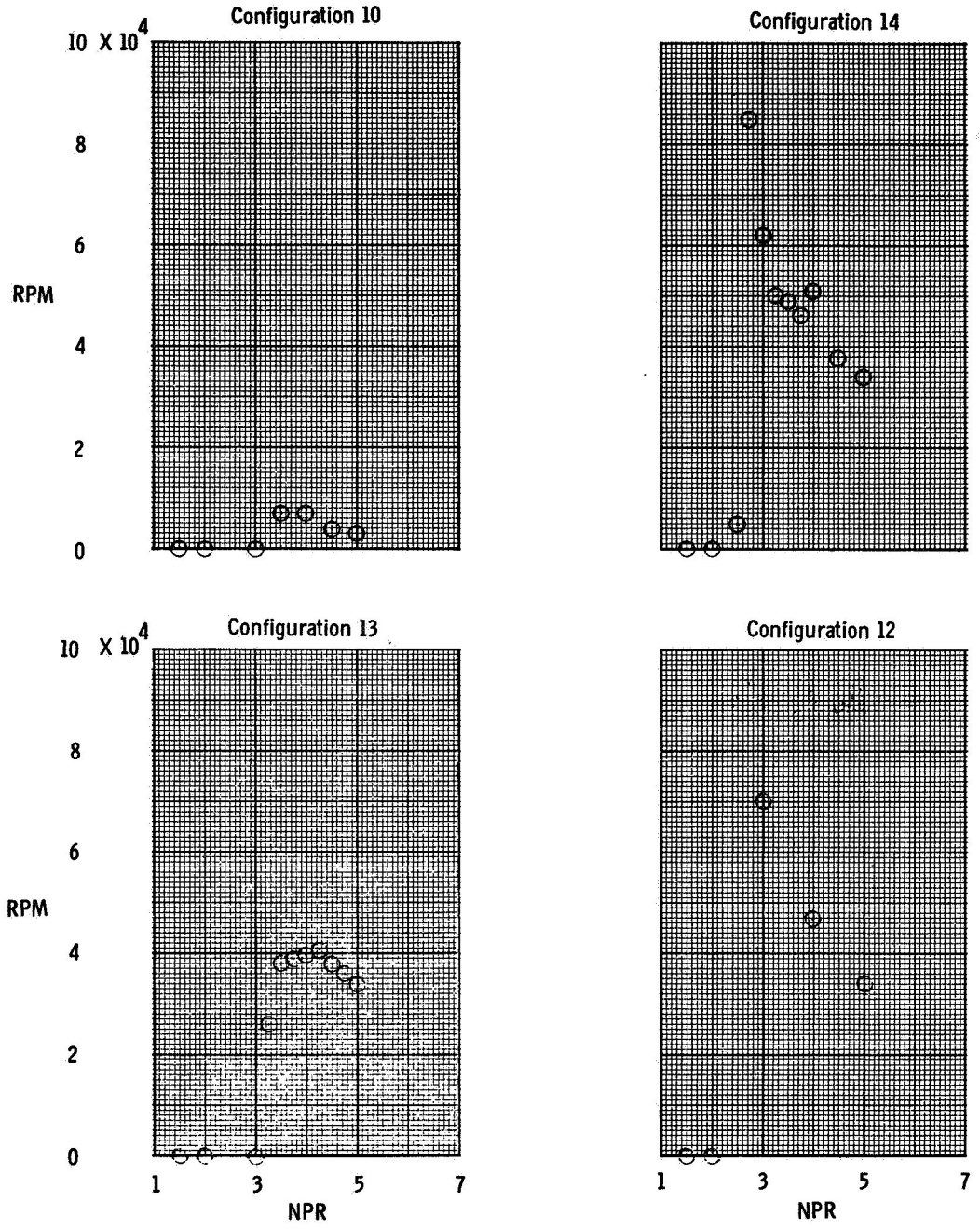

Figure 7. Variation of cylinder revolutions per minute(RPM) with nozzle pressure ratio(NPR) for self-propelled, rotating cylinder configurations.

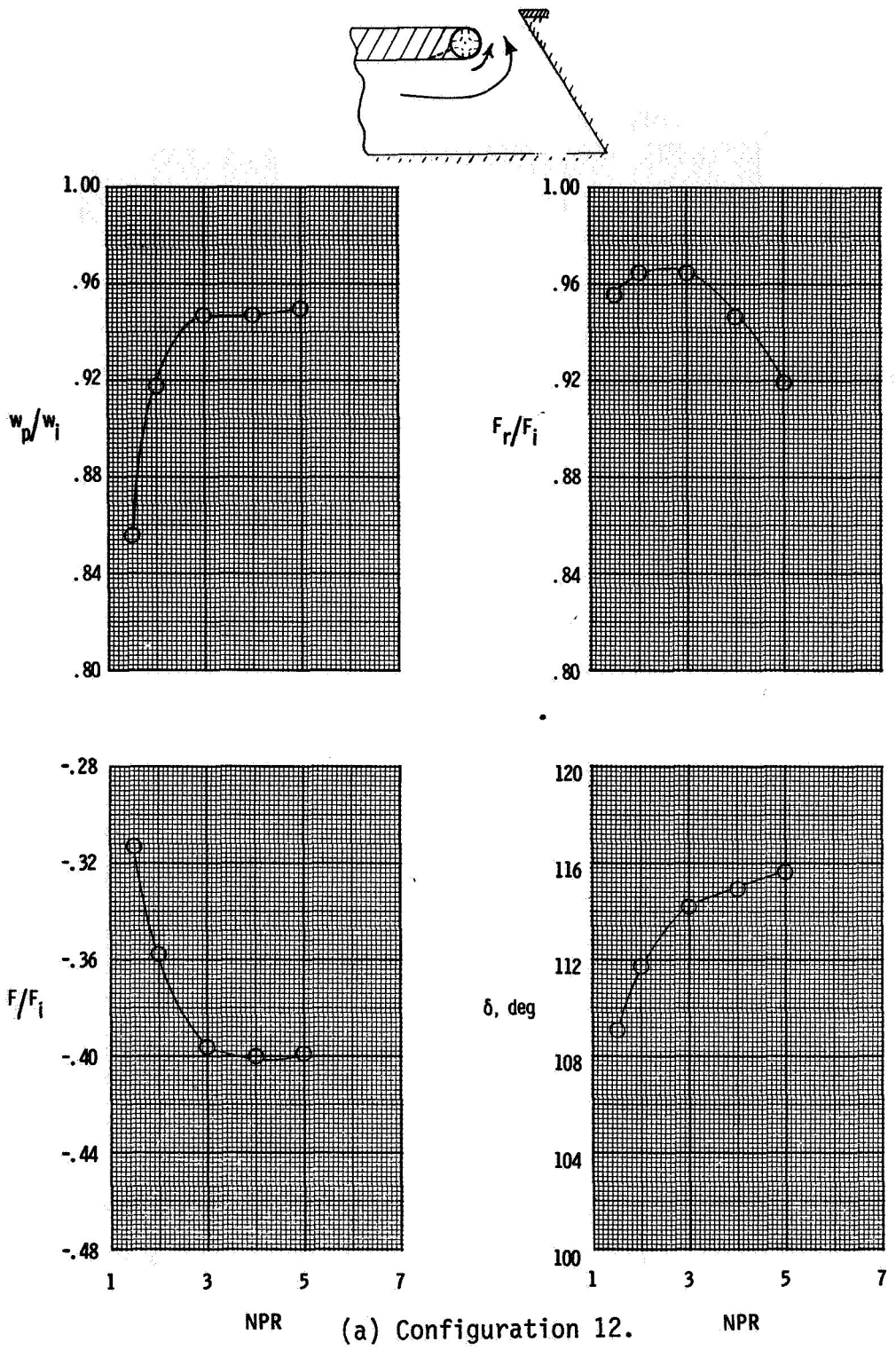

(a) Configuration 12.

Figure 8. Variation of discharge coefficient(w_p/w_i), resultant gross thrust ratio(F_r/F_i), axial thrust ratio(F/F_i), and thrust vector angle(δ) with nozzle pressure ratio(NPR) for 0.250 inch radius self-propelled, rotating cylinder configurations.

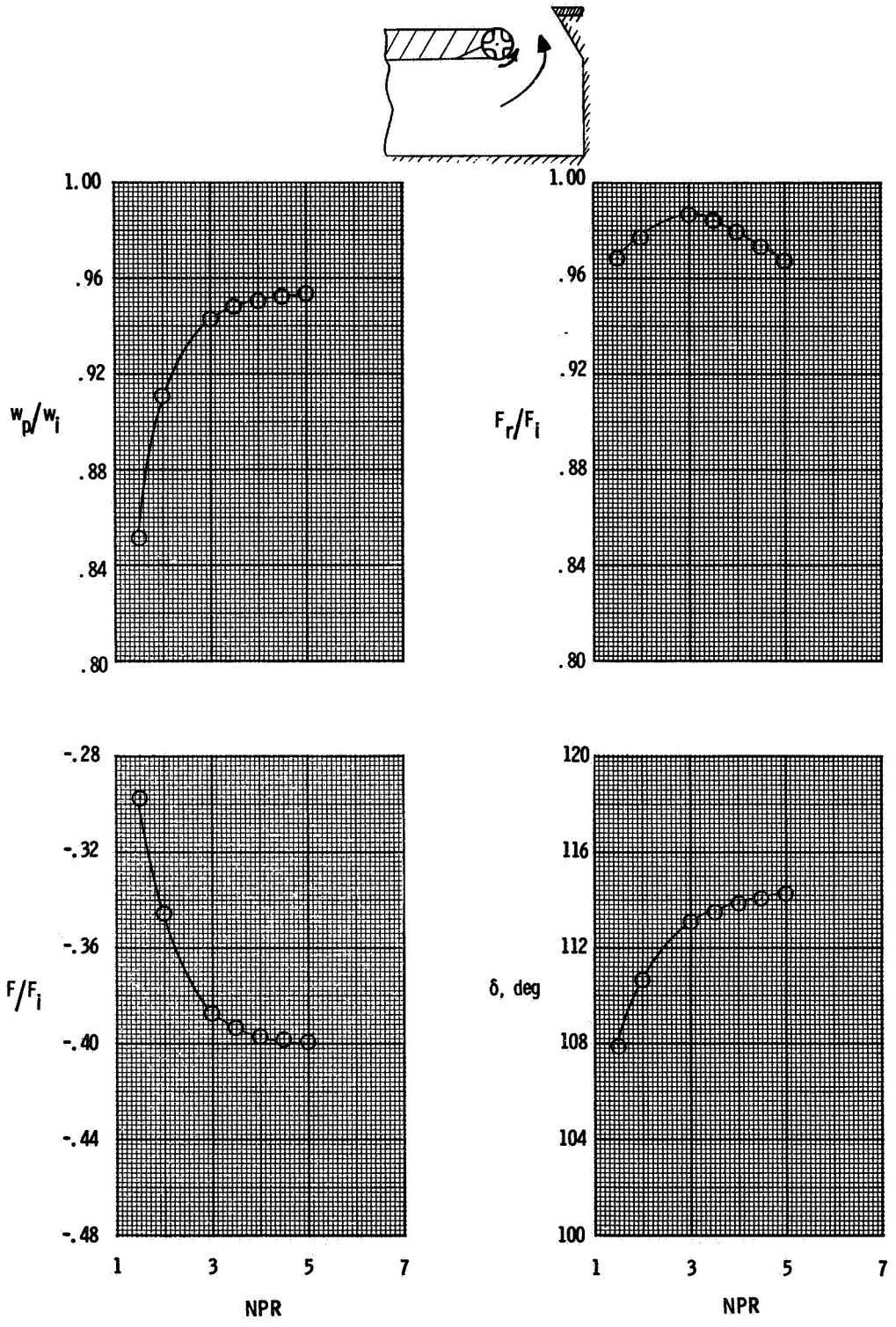

(b) Configuration 10.

Figure 8. Continued.

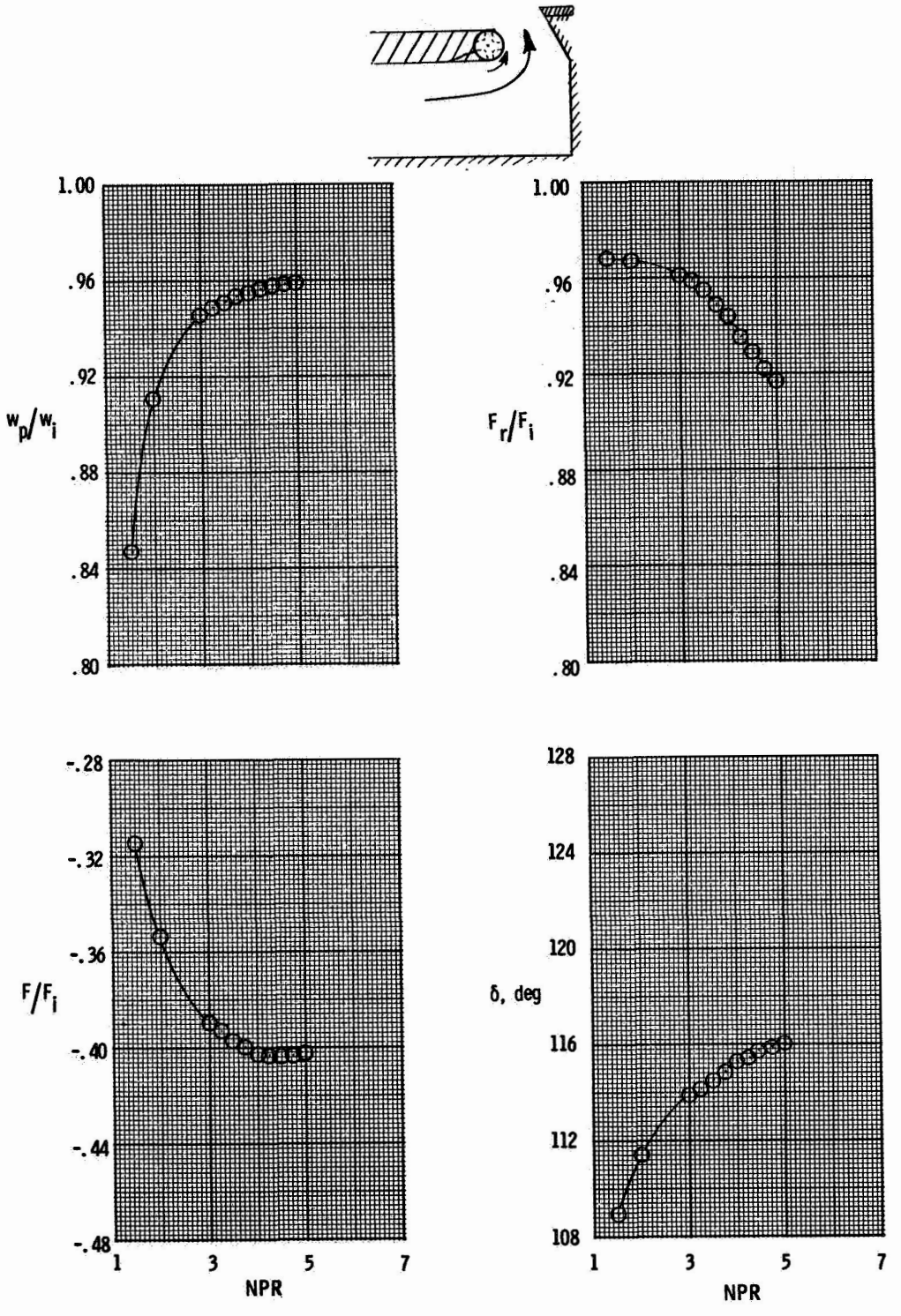

(c) Configuration 13.

Figure 8. Continued.

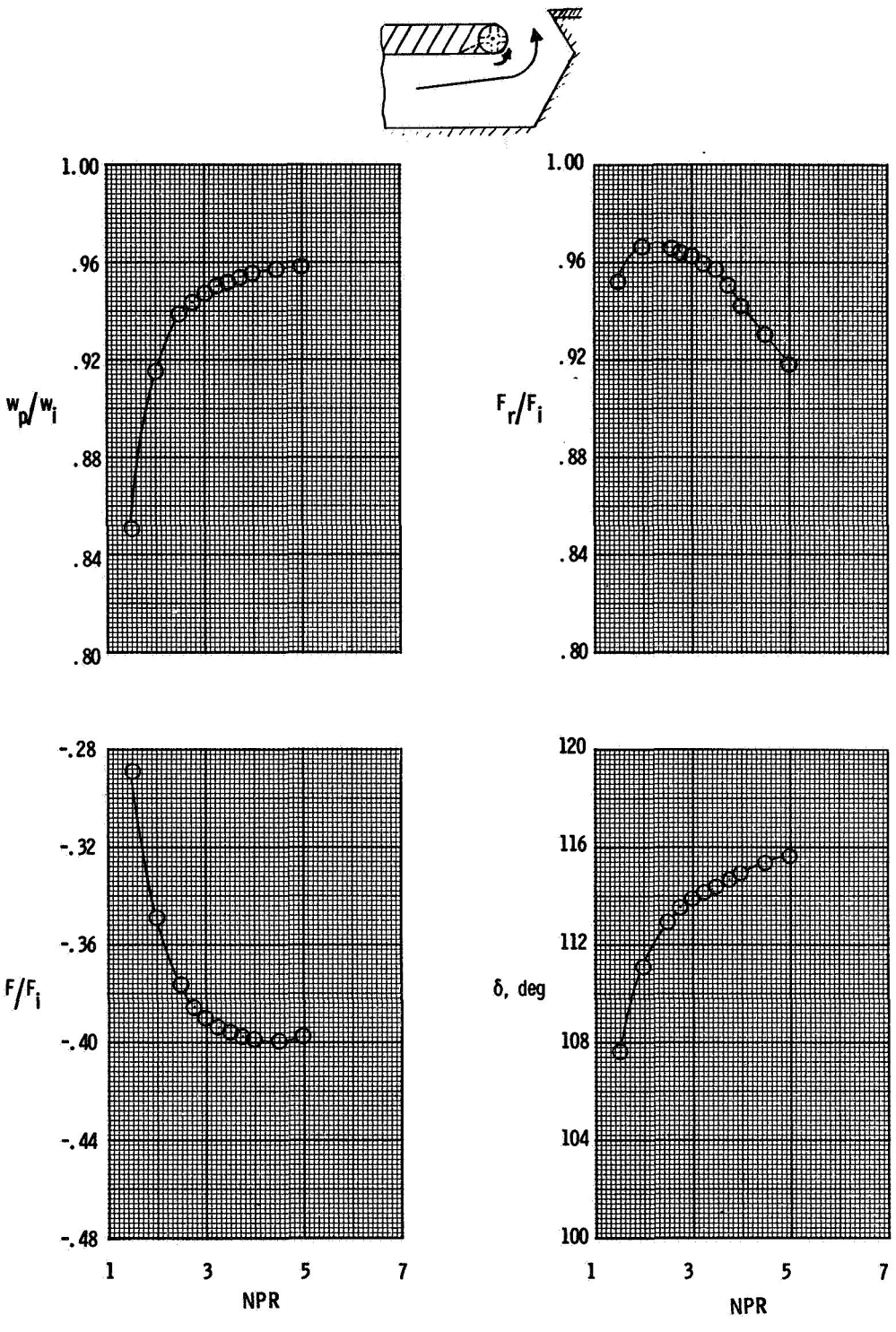

(d) Configuration 14.

Figure 8. Concluded.

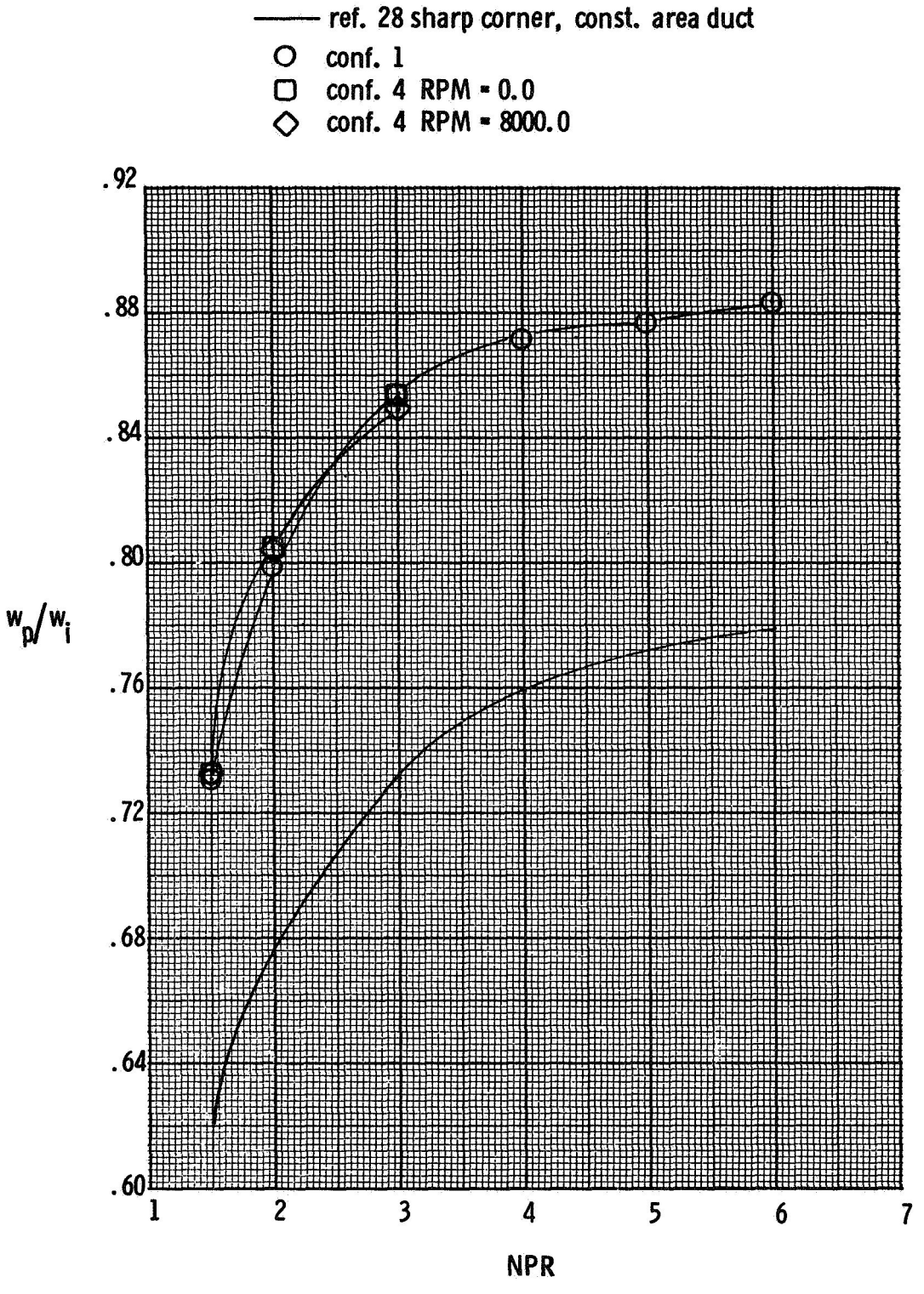

(a) Constant area duct.

Figure 9. Effect of corner shape and cylinder rotation on discharge coefficient(w_p/w_i).

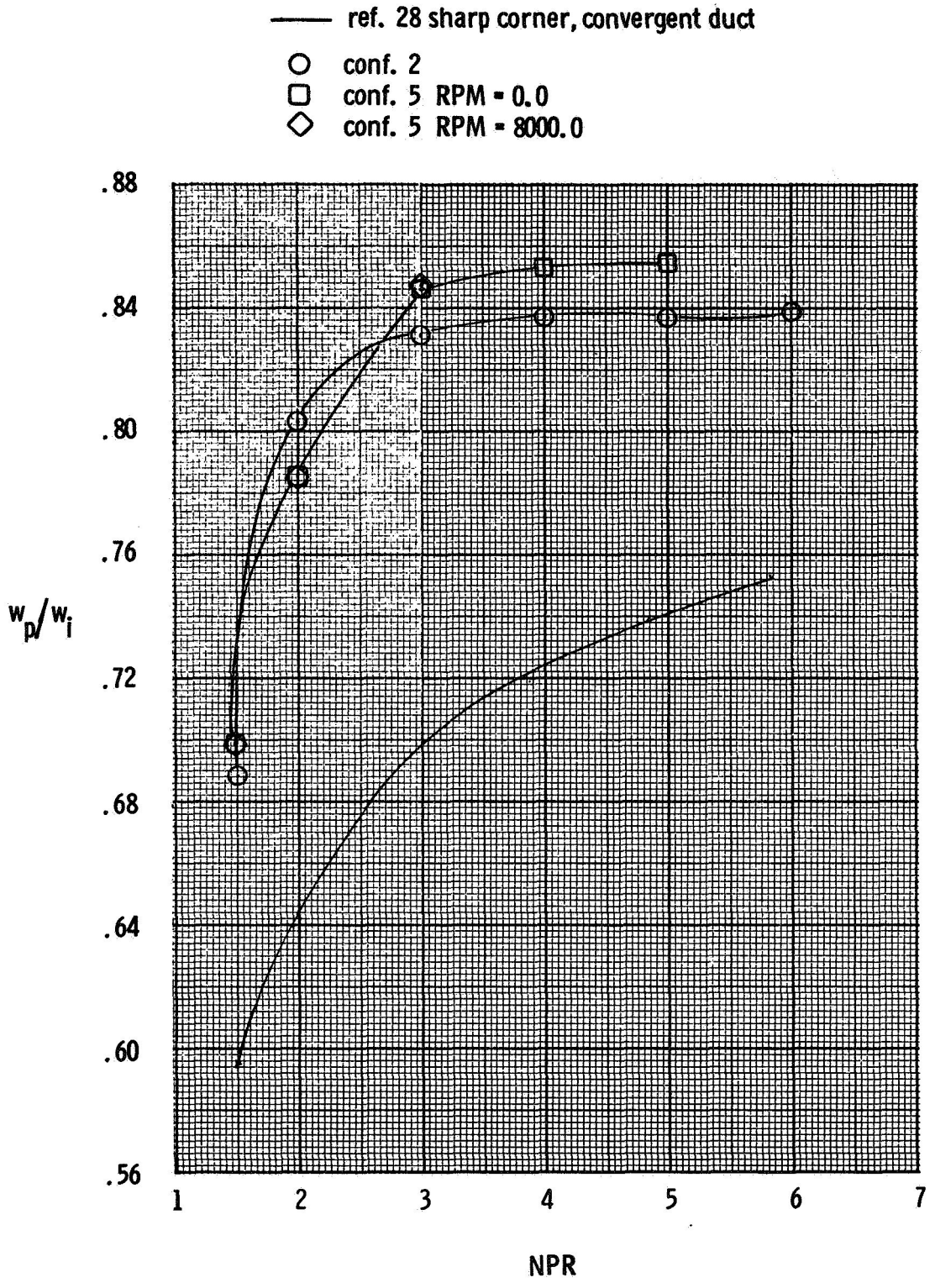

(b) Convergent duct, 0.491 inch port passage length.

Figure 9. Continued.

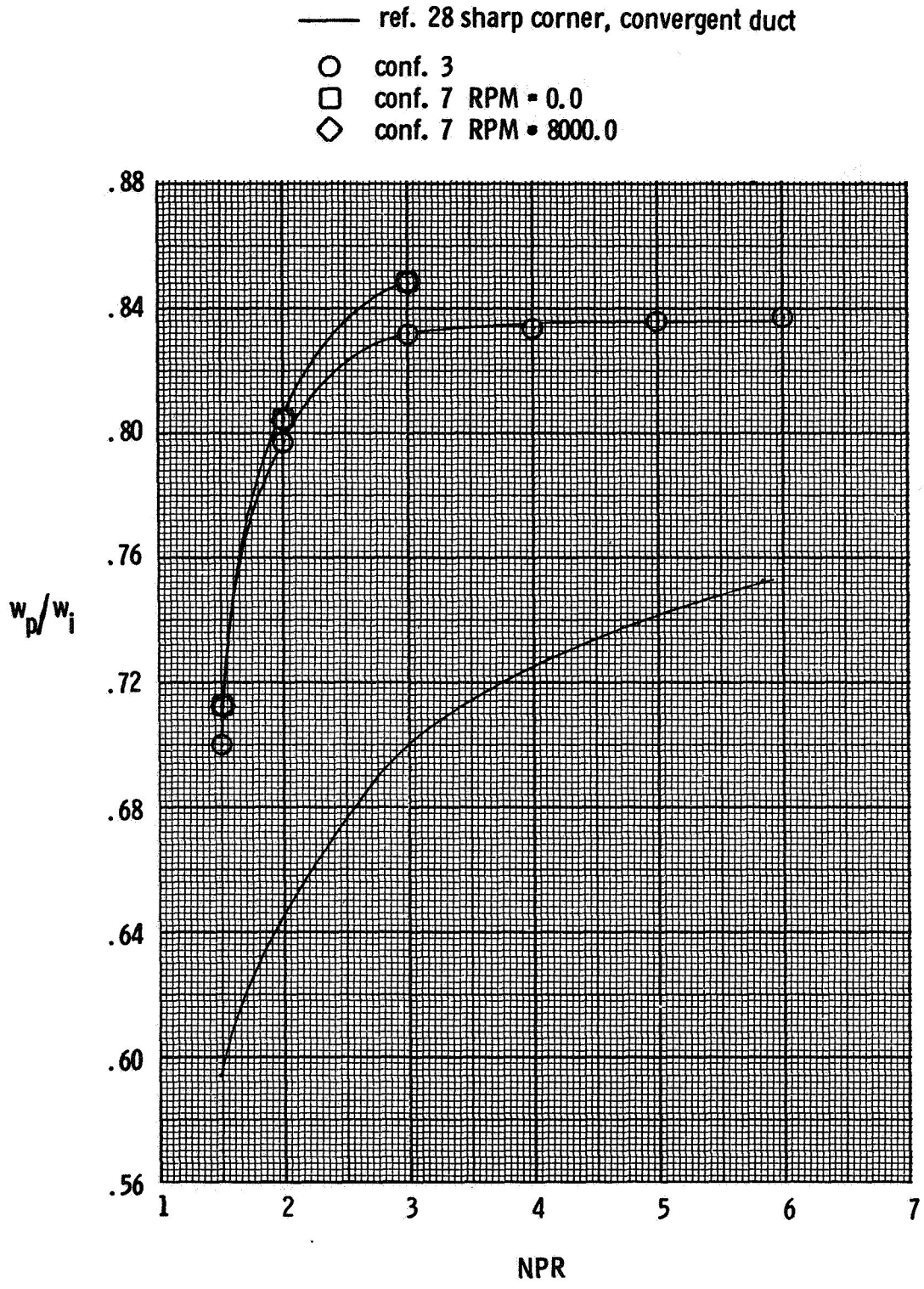

(c) Convergent duct, nominal port passage length of 0.66 inches.

Figure 9. Concluded.

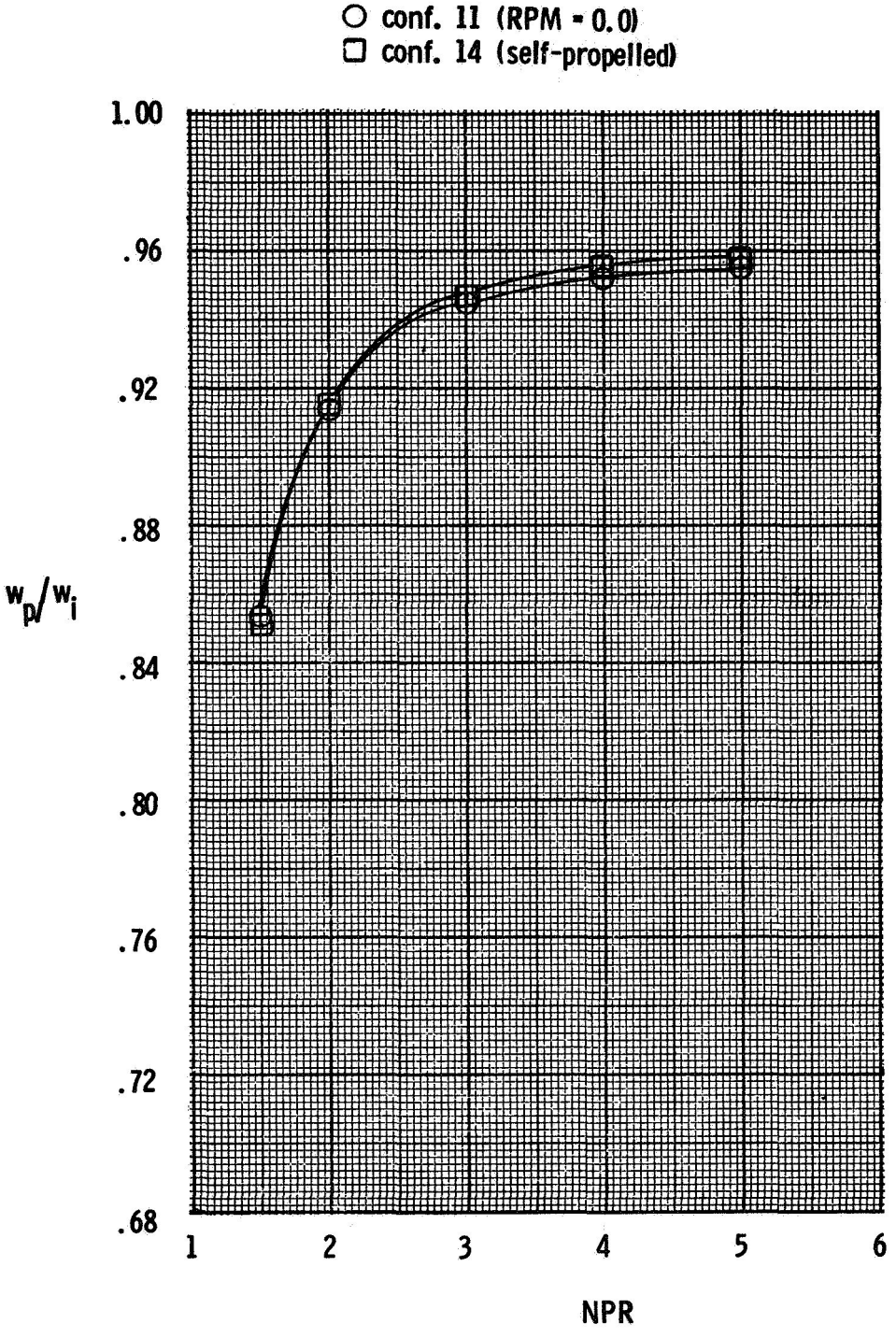

Figure 10. Effect of cylinder rotation on discharge coefficient(w_p/w_i) for a self propelled, rotating cylinder configuration.

1. Report No.	2. Government Accession No.	3. Recipient's Catalog No.
NASA CR-178036		

4. Title and Subtitle	5. Report Date
AN INVESTIGATION AT STATIC CONDITIONS OF NONAXISYMMETRIC NOZZLE THRUST REVERSER PORT GEOMETRY INCLUDING EFFECTS OF ROUNDING AND ROTATING THE PORT CORNER	November 1985
	6. Performing Organization Code
7. Author(s)	8. Performing Organization Report No.
Dorothy G. Arbiter	
	10. Work Unit No.
9. Performing Organization Name and Address	11. Contract or Grant No.
Vigyan Research Associates, Inc. 28 Research Drive Hampton, VA 23666	NAS1-17919
	13. Type of Report and Period Covered
12. Sponsoring Agency Name and Address	Contractor Report
National Aeronautics and Space Administration Washington, DC 20546	14. Sponsoring Agency Code 505-62-91-01

15. Supplementary Notes

Langley Technical Monitor: William P. Henderson

16. Abstract

An investigation has been conducted in the static test facility of the Langley 16-Foot Transonic Tunnel to determine the effects of rounding and rotating the port corner of a nonaxisymmetric thrust reversing port. High pressure air was used to simulate jet exhaust at nozzle pressure ratios up to 6.0.

The results of this investigation indicate that using a rounded corner in the reverser port passage increased the discharge coefficient significantly compared to that of a sharp cornered thrust reversing port. Incorporating a rotating cylinder into the rounded corner reverser port passage provided no additional increase at cylinder revolutions per minute up to 10,000. (Revolutions per minute of 390,000 were necessary to achieve a surface velocity equal to the duct velocity.) Highest levels of discharge coefficient were obtained by providing a large, round, cylindrical surface in the port upstream wall. Locating the reverser port in a constant area duct resulted in higher discharge coefficients than locating the port in a convergent duct.

17. Key Words (Suggested by Author(s))	18. Distribution Statement
rotating cylinder thrust reverser static test single port nonaxisymmetric thrust reversing port	Unclassified-Unlimited Subject Category 02

19. Security Classif. (of this report)	20. Security Classif. (of this page)	21. No. of Pages	22. Price
Unclassified	Unclassified	55	A04

For sale by the National Technical Information Service, Springfield, Virginia 22161